3.2 Numerical Simulation of Marangoni Convection in Consideration of Free Surface Displacement (Part 3)

Hiroshi Kawamura

Science University of Tokyo

NUMERICAL SIMULATION OF MARANGONI CONVECTION IN CONSIDERATION OF FREE SURFACE DISPLACEMENT(PART 3)

Yoshiki Kaizu*, Masayuki Goto*, Ichiro Ueno* and Hiroshi Kawamura*

*Science University of Tokyo, 2641 Yamazaki, Noda-shi, Chiba 278-8510, Japan

Abstract

One of the purposes of the space environment utilization such as a space station is the process of a new material. Uniform or high-quality material can be formed on the ground owing to the natural convection by the buoyancy effect and sedimentation by the density difference. On the other hand, the buoyancy effect can be reduced in the space environment. Thus a high-quality material processing is expected to be enabled.

Floating Zone Method is one of the likely candidates of the material processing methods under the micro-gravity. In this method the both ends of the material rod are cooled down, and the center is heated to melt. Molten liquid sustained between the rods is called liquid bridge. This melt zone is slowly moved vertically and thus a uniform single crystal is produced. The material in the liquid phase is sustained by the surface tension. Generally the surface tension of a liquid decreases with increasing temperature. Because a temperature variation exists along the free surface, the difference of the surface tension is originated from the temperature difference. Thus a flow occurs in a liquid bridge even under the micro-gravity. This flow is called as thermocapillary or Marangoni convection. Though this convection can occur also on the ground, it is usually hidden in the action of the buoyancy. And this phenomenon is hardly recognized in our usual observation. On the other hand, thermocapillary convection becomes dominant under the micro-gravity because the influence of the buoyancy is strongly reduced. Therefore, the analysis of the thermocapillary convection is primary important for the material formation under the micro-gravity. The configuration of the floating zone method is called as Full Zone Model. For the sake of simplicity, Half Zone Model is preferred in the fundamental research on the ground. Half zone model is the part of the liquid bridge in the full zone model. In this study, the upper disk is heated up and the other one is cooled down.

From existing researches, thermocapillary convection exhibits the oscillatory flow under a certain condition. And the free surface vibration is observed with the oscillatory flow in the terrestrial experiments. An influence of surface vibration upon the flow field instability must be evaluated to understand the mechanism of the oscillatory flow. However existing numerical simulation are performed without considering the free surface movement.

Consequently the purpose of this research is to analyze the three dimensional thermocapillary convection numerically with consideration of the free surface movement. The numerical analysis of thermocapillary convection was performed by the finite difference method using boundary fitted coordinate. The free surface deformation was considered in this calculation. As the results, the free surface deformation is obtained from the beginning of the thermocapillary convection to the steady one. The cases of different Marangoni number are calculated and its influence on the thermocapillary convection are analyzed.

1 INTRODUCTION

One of the purposes of the space environment utilization such as a space station is the production of a new material. Uniform or high-quality material can rather hardly be formed on the ground owing to the natural convection by the buoyancy effect and sedimentation by the density difference. On the other hand, the buoyancy effect can be reduced and thus, a high-quality material processing is expected to be enabled in the space environment.

Floating Zone Method is one of the likely candidates of the material processing methods under the micro-gravity. In this method the both ends of the material rod are cooled down, and the center is heated to be melt. Molten liquid sustained between the rods is called a liquid bridge. This melt zone is slowly moved vertically and thus a uniform single crystal is produced. The material in the liquid phase is sustained by the surface tension. Generally the surface tension of a liquid decreases with increasing temperature. Because a temperature gradient exists along the free surface, the difference of the surface tension is originated by the temperature difference. Thus a flow occurs in a liquid bridge even under the micro-gravity. This flow is called as thermocapillary or Marangoni convection. Though this convection can occur also on the ground, it is usually hidden by the buoyancy. Thus this phenomenon is hardly recognized in our usual observation. On the other hand, thermocapillary convection becomes dominant under the micro-gravity because the influence of the buoyancy is strongly reduced. Therefore, the analysis of the thermocapillary convection is of primary importance for the material formation under the micro-gravity. The configuration of the floating zone method is called as Full Zone Model. The upper half of the full zone model is deeply influenced by the buoyancy on the ground so that the thermocapillary effect can scarcely be recognized. On the other hand, the lower half is less affected by buoyancy. Because upper temperature is higher than the lower one. As the results the thermocapillary effect dominates the convection in the lower half of the full zone model. Consequently Half Zone Model is preferred in the fundamental research on the ground and is employed in this research as well. The half zone model corresponds to the half part of the liquid bridge in the full zone model; the one side of the bridge is heated up and the other is cooled down.

The experiments for the thermocapillary convention are widely conducted. Kamotani[1]studied effect of zone rotation on oscillatory thermocapillary flow in simulated floating zones. Velten[2] observed the periodic instability of thermocapillary convection in cylindrical liquid bridges.

As for the numerical simulation Savino and Monti[3] simulated the oscillatory flow numerically and compared it with their experiments. Yasuhiro[4] investigated the relations between the wave number and aspect ratio or Marangoni number.

From these researches, it turned out that thermocapillary convection exhibits the oscillatory flow under a certain condition.

It should be noted that the existing numerical simulations ware conducted without considering the free surface movement. On the other hand, the free surface vibration is observed with the oscillatory flow in the terrestrial experiments. An influence of surface vibration upon the flow field instability must be evaluated to understand the mechanism of the oscillatory flow.

Consequently the purpose of this research is to analyze the three dimensional thermocapillary convection numerically with consideration of the free surface movement.

2 NOMENCLATURE

D	diameter
g	gravity
H	height of the liquid bridge
$\mathbf{I}$	unit matrix
J	Jacobian
$\mathbf{n}$	surface-normal vector
N	normalizing dominator
P	pressure
r, θ, z	coordinates
R, R_k	position of the free surface
R_0	radius of the disk
$R_{1,2}$	main radii of curvature
$\mathbf{S}$	stress tensor
t	time
T	temperature
T_0	reference temperature
$v_{r,\theta,z}, V_{x,y}$	velocities
$\hat{v}_i$	velocity without considering the movement of the computational grid
$\tilde{v}_i$	temporally velocity
V	volume of the liquid bridge
$V_{\xi,\zeta,\eta}$	contravariant velocities
$\tilde{V}_{\xi,\zeta,\eta}$	temporally contravariant velocities
ΔT	temperature difference between the disks
λ	coefficient of viscosity
μ	dynamic viscosity
ν	kinematic viscosity
ξ, ζ, η	coordinates in the computational domain
rho	density
$\sigma, \sigma(T)$	surface tension
$\sigma_0(T_0)$	reference surface tension
σ_T	thermal coefficient of surface tension
τ	time in the computational domain
$\varphi, \theta_{v\theta vr}$	angle
Bo	Bond number
Ca	Capillary number
Gr	Grashof number
Ma	Marangoni number
Pr	Prandtl number
Re	Reynolds number

3 NUMERICAL METHOD FOR THE THREE DIMENSIONAL ANALYSIS

The goal of this study is to analyze the influence of the free surface deformation upon the thermocapillary flow. Therefore, an analytical method is developed to capture the temporally varing surface motion. In this analysis, B.F.C.(Boundary Fitted Coordinate) method is employed.

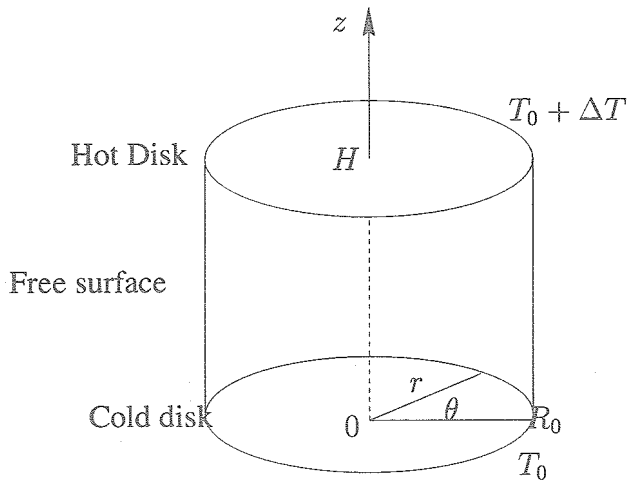

Figure 1: The configuration

To consider a thermocapillary convection in a liquid bridge, a configuration of the analysis is defined in figure 1. The liquid bridge with volume V is bounded by two rigid parallel disks of equal radii $r = R_0$ located at $z = 0$ and H. The temperature difference between these disks is defined by ΔT. The gravity is assumed in the direction of $-z$.
The governing equations are described in cylindrical coordinate. As for the gravity, the Oberbeck-Boussinesq approximation is utilized in these equations.

3.1 The governing equation

[Continuity equation]

$$\frac{\partial}{\partial r}(rv_r) + \frac{\partial v_\theta}{\partial \theta} + \frac{\partial}{\partial z}(rv_z) = 0 \tag{1}$$

[Navier-Stokes equation]
(r-direction)

$$r\frac{\partial v_r}{\partial t} + \frac{\partial}{\partial r}(rv_r v_r) + \frac{\partial}{\partial \theta}(v_\theta v_r) - v_\theta^2 + \frac{\partial}{\partial z}(rv_z v_r) = -r\frac{\partial P}{\partial r}$$
$$+\frac{Pr}{Ma}[\frac{\partial}{\partial r}(r\frac{\partial v_r}{\partial r}) + \frac{\partial}{\partial \theta}(\frac{1}{r}\frac{\partial v_r}{\partial \theta}) + \frac{\partial}{\partial z}(r\frac{\partial v_r}{\partial z}) - \frac{v_r}{r} - \frac{2}{r}\frac{\partial v_\theta}{\partial \theta}]$$

(θ-direction)

$$r\frac{\partial v_\theta}{\partial t} + \frac{\partial}{\partial r}(rv_r v_\theta) + \frac{\partial}{\partial \theta}(v_\theta v_\theta) - v_r v_\theta + \frac{\partial}{\partial z}(rv_z v_\theta) = -\frac{\partial P}{\partial \theta}$$
$$+\frac{Pr}{Ma}[\frac{\partial}{\partial r}(r\frac{\partial v_\theta}{\partial r}) + \frac{\partial}{\partial \theta}(\frac{1}{r}\frac{\partial v_\theta}{\partial \theta}) + \frac{\partial}{\partial z}(r\frac{\partial v_\theta}{\partial z}) + \frac{2}{r}\frac{\partial v_r}{\partial \theta} - \frac{v_\theta}{r}]$$

(z-direction)

$$r\frac{\partial v_z}{\partial t} + \frac{\partial}{\partial r}(rv_r v_z) + \frac{\partial}{\partial \theta}(v_\theta v_z) + \frac{\partial}{\partial z}(rv_z v_z) = -\frac{\partial P}{\partial z}$$

$$+\frac{Pr}{Ma}[\frac{\partial}{\partial r}(r\frac{\partial v_z}{\partial r})+\frac{\partial}{\partial \theta}(\frac{1}{r}\frac{\partial v_z}{\partial \theta})+\frac{\partial}{\partial z}(r\frac{\partial v_z}{\partial z})]$$
$$+\frac{Gr}{Re^2}T \tag{2}$$

[Energy equation]

$$r\frac{\partial T}{\partial t}+\frac{\partial}{\partial r}(rv_rT)+\frac{\partial}{\partial \theta}(v_\theta T)+\frac{\partial}{\partial z}(rv_zT)$$
$$=\frac{1}{Ma}[\frac{\partial}{\partial r}(r\frac{\partial T}{\partial r})+\frac{\partial}{\partial \theta}(\frac{1}{r}\frac{\partial T}{\partial \theta})+\frac{\partial}{\partial z}(r\frac{\partial T}{\partial z})] \tag{3}$$

The scales used for non-dimensionalization are as follows.

Table 1: Scales used for non-dimensionalization

Variable	r, z	t	$\mathrm{v}=(v_r, v_\theta, v_z)$	p	T
Scale	H	$H\mu/\sigma_T\Delta T$	$\sigma_T\Delta T/\mu$	$\rho(\sigma_T\Delta T/\mu)^2$	ΔT

The non-dimensional numbers are defined by

$$Re = \frac{vH}{\nu}$$
$$Pr = \frac{\nu}{\kappa}$$
$$Ma = \frac{1}{\mu\kappa}\sigma_T\Delta T\cdot H$$
$$Gr = \frac{g\beta\Delta T H^3}{\nu^2}$$

Eqs. (1)-(3) can be transformed from the physical domain to the computational domain by Jacobian matrix.

$$\begin{bmatrix} \frac{\partial}{\partial t} \\ \frac{\partial}{\partial r} \\ \frac{\partial}{\partial \theta} \\ \frac{\partial}{\partial z} \end{bmatrix} = \begin{bmatrix} 1 & \xi_t & \zeta_t & \eta_t \\ 0 & \xi_r & \zeta_r & \eta_r \\ 0 & \xi_\theta & \zeta_\theta & \eta_\theta \\ 0 & \xi_z & \zeta_z & \eta_z \end{bmatrix} \begin{bmatrix} \frac{\partial}{\partial \tau} \\ \frac{\partial}{\partial \xi} \\ \frac{\partial}{\partial \zeta} \\ \frac{\partial}{\partial \eta} \end{bmatrix} \tag{4}$$

$$\begin{bmatrix} \frac{\partial}{\partial \tau} \\ \frac{\partial}{\partial \xi} \\ \frac{\partial}{\partial \zeta} \\ \frac{\partial}{\partial \eta} \end{bmatrix} = \begin{bmatrix} 1 & r_\tau & \theta_\tau & z_\tau \\ 0 & r_\xi & \theta_\xi & z_\xi \\ 0 & r_\zeta & \theta_\zeta & z_\zeta \\ 0 & r_\eta & \theta_\eta & z_\eta \end{bmatrix} \begin{bmatrix} \frac{\partial}{\partial t} \\ \frac{\partial}{\partial r} \\ \frac{\partial}{\partial \theta} \\ \frac{\partial}{\partial z} \end{bmatrix} \tag{5}$$

Equation (5) is inversely transformed as follows,

$$\begin{bmatrix} \frac{\partial}{\partial t} \\ \frac{\partial}{\partial r} \\ \frac{\partial}{\partial \theta} \\ \frac{\partial}{\partial z} \end{bmatrix} = \frac{1}{J}\begin{bmatrix} A_{11} & A_{12} & A_{13} & A_{14} \\ A_{21} & A_{22} & A_{23} & A_{24} \\ A_{31} & A_{32} & A_{33} & A_{34} \\ A_{41} & A_{42} & A_{43} & A_{44} \end{bmatrix} \begin{bmatrix} \frac{\partial}{\partial \tau} \\ \frac{\partial}{\partial \xi} \\ \frac{\partial}{\partial \zeta} \\ \frac{\partial}{\partial \eta} \end{bmatrix} \tag{6}$$

$$
\begin{aligned}
A_{11} &= (r_\xi\theta_\zeta z_\eta + r_\zeta\theta_\eta z_\xi + r_\eta\theta_\xi z_\zeta - r_\eta\theta_\zeta z_\xi - r_\zeta\theta_\xi z_\eta - r_\xi\theta_\eta z_\zeta)\\
A_{12} &= -(r_\tau\theta_\zeta z_\eta + r_\zeta\theta_\eta z_\tau + r_\eta\theta_\tau z_\zeta - r_\eta\theta_\zeta z_\tau - r_\zeta\theta_\tau z_\eta - r_\tau\theta_\eta z_\zeta)\\
A_{13} &= (r_\tau\theta_\xi z_\eta + r_\xi\theta_\eta z_\tau + r_\eta\theta_\tau z_\xi - r_\eta\theta_\xi z_\tau - r_\xi\theta_\tau z_\eta - r_\tau\theta_\eta z_\xi)\\
A_{14} &= -(r_\tau\theta_\xi z_\zeta + r_\xi\theta_\zeta z_\tau + r_\zeta\theta_\tau z_\xi - r_\zeta\theta_\xi z_\tau - r_\xi\theta_\tau z_\zeta - r_\tau\theta_\zeta z\xi)\\
A_{21} &= 0\\
A_{22} &= (\theta_\zeta z_\eta - \theta_\eta z_\zeta)\\
A_{23} &= -(\theta_\xi z_\eta - \theta_\eta z_\xi)\\
A_{24} &= (\theta_{xi} z\zeta - \theta_\zeta z_\xi)\\
A_{31} &= 0\\
A_{32} &= -(r_\zeta z_\eta - r_\eta z_\zeta)\\
A_{33} &= (r_\xi z_\eta - r_\eta z_\xi)\\
A_{34} &= -(r_\xi z_\zeta - r_\zeta z_\xi)\\
A_{41} &= 0\\
A_{42} &= (r_\zeta\theta_\eta - r_\eta\theta_\zeta)\\
A_{43} &= -(r_\xi\theta_\eta - r_\eta\theta_\xi)\\
A_{44} &= (r_\xi\theta_\zeta - r_\zeta\theta_\xi)
\end{aligned}
$$

Each component can be related from Eqs. (4), (6) as:

$$
\begin{aligned}
J &= r_\xi\theta_\zeta z_\eta + r_\zeta\theta_\eta z_\xi + r_\eta\theta_\xi z_\zeta - r_\eta\theta_\zeta z_\xi - r_\zeta\theta_\xi z_\eta - r_\xi\theta_\eta z_\zeta\\
\xi_t &= -\frac{1}{J}(r_\tau\theta_\zeta z_\eta + r_\zeta\theta_\eta z_\tau + r_\eta\theta_\tau z_\zeta - r_\eta\theta_\zeta z_\tau - r_\zeta\theta_\tau z_\eta - r_\tau\theta_\eta z_\zeta)\\
\zeta_t &= \frac{1}{J}(r_\tau\theta_\xi z_\eta + r_\xi\theta_\eta z_\tau + r_\eta\theta_\tau z_\xi - r_\eta\theta_\xi z_\tau - r_\xi\theta_\tau z_\eta - r_\tau\theta_\eta z_\xi)\\
\eta_t &= -\frac{1}{J}(r_\tau\theta_\xi z_\zeta + r_\xi\theta_\zeta z_\tau + r_\zeta\theta_\tau z_\xi - r_\zeta\theta_\xi z_\tau - r_\xi\theta_\tau z_\zeta - r_\tau\theta_\zeta z\xi)\\
\xi_r &= \frac{1}{J}(\theta_\zeta z_\eta - \theta_\eta z_\zeta)\\
\zeta_r &= -\frac{1}{J}(\theta_\xi z_\eta - \theta_\eta z_\xi)\\
\eta_r &= \frac{1}{J}(\theta_{xi} z\zeta - \theta_\zeta z_\xi)\\
\xi_\theta &= -\frac{1}{J}(r_\zeta z_\eta - r_\eta z_\zeta)\\
\zeta_\theta &= \frac{1}{J}(r_\xi z_\eta - r_\eta z_\xi)\\
\eta_\theta &= -\frac{1}{J}(r_\xi z_\zeta - r_\zeta z_\xi)\\
\xi_z &= \frac{1}{J}(r_\zeta\theta_\eta - r_\eta\theta_\zeta)\\
\zeta_z &= -\frac{1}{J}(r_\xi\theta_\eta - r_\eta\theta_\xi)\\
\eta_z &= \frac{1}{J}(r_\xi\theta_\zeta - r_\zeta\theta_\xi) \quad .
\end{aligned}
$$

The continuity equation, the Navier-Stokes equation and the energy equation (Eqs. (1)-(3)) are

transformed by these rules.
[Continuity equation]

$$\frac{\partial}{\partial\xi}(JrV_\xi)+\frac{\partial}{\partial\zeta}(JrV_\zeta)+\frac{\partial}{\partial\eta}(JrV_\eta)=0 \tag{7}$$

Here, V_ξ, V_ζ, V_η are defined by

$$\begin{aligned} V_\xi &= \xi_r v_r+\frac{1}{r}\xi_\theta v_\theta+\xi_z v_z \\ V_\zeta &= \zeta_r v_r+\frac{1}{r}\zeta_\theta v_\theta+\zeta_z v_z \\ V_\eta &= \eta_r v_r+\frac{1}{r}\eta_\theta v_\theta+\eta_z v_z\ . \end{aligned}$$

These velocities are called as **contravariant velocities.**
[Navier-Stokes equation]

$$\frac{\partial v_i}{\partial t}+(v_i\cdot\nabla)\cdot v_i=\nabla P+\frac{Pr}{Ma}\nabla^2\cdot v_i+e_z\frac{Gr}{Re^2}T \tag{8}$$

Equation (8) is expanded as

$$\begin{aligned} &\frac{\partial v_i}{\partial t}+\xi_t\frac{\partial v_i}{\partial\xi}+\zeta_t\frac{\partial v_i}{\partial\zeta}+\eta_t\frac{\partial v_i}{\partial\eta} \\ &+\frac{1}{Jr}\left[\frac{\partial}{\partial\xi}(JrV_\xi v_i)+\frac{\partial}{\partial\zeta}(JrV_\zeta v_i)+\frac{\partial}{\partial\eta}(JrV_\eta v_i)+e_r\Big(-Jv_\theta^2\Big)+e_\theta\Big(Jv_r v_\theta\Big)\right] \\ = \quad &-\Big(\xi_i\frac{\partial P}{\partial\xi}+\zeta_i\frac{\partial P}{\partial\zeta}+\eta_i\frac{\partial P}{\partial\eta}\Big)e_i \\ +\tfrac{Pr}{Ma}\tfrac{1}{Jr}\Big[\ &\frac{\partial}{\partial\xi}(Jr\xi_r\xi_r\frac{\partial v_i}{\partial\xi})+\frac{\partial}{\partial\xi}(Jr\xi_r\zeta_r\frac{\partial v_i}{\partial\zeta})+\frac{\partial}{\partial\xi}(Jr\xi_r\eta_r\frac{\partial v_i}{\partial\eta}) \\ +\ &\frac{\partial}{\partial\zeta}(Jr\zeta_r\xi_r\frac{\partial v_i}{\partial\xi})+\frac{\partial}{\partial\zeta}(Jr\zeta_r\zeta_r\frac{\partial v_i}{\partial\zeta})+\frac{\partial}{\partial\zeta}(Jr\zeta_r\eta_r\frac{\partial v_i}{\partial\eta}) \\ +\ &\frac{\partial}{\partial\eta}(Jr\eta_r\xi_r\frac{\partial v_i}{\partial\xi})+\frac{\partial}{\partial\eta}(Jr\eta_r\zeta_r\frac{\partial v_i}{\partial\zeta})+\frac{\partial}{\partial\eta}(Jr\eta_r\eta_r\frac{\partial v_i}{\partial\eta}) \\ +\ &\frac{\partial}{\partial\xi}(J\frac{1}{r}\xi_\theta\xi_\theta\frac{\partial v_i}{\partial\xi})+\frac{\partial}{\partial\xi}(J\frac{1}{r}\xi_\theta\zeta_\theta\frac{\partial v_i}{\partial\zeta})+\frac{\partial}{\partial\xi}(J\frac{1}{r}\xi_\theta\eta_\theta\frac{\partial v_i}{\partial\eta}) \\ +\ &\frac{\partial}{\partial\zeta}(J\frac{1}{r}\zeta_\theta\xi_\theta\frac{\partial v_i}{\partial\xi})+\frac{\partial}{\partial\zeta}(J\frac{1}{r}\zeta_\theta\zeta_\theta\frac{\partial v_i}{\partial\zeta})+\frac{\partial}{\partial\zeta}(J\frac{1}{r}\zeta_\theta\eta_\theta\frac{\partial v_i}{\partial\eta}) \\ +\ &\frac{\partial}{\partial\eta}(J\frac{1}{r}\eta_\theta\xi_\theta\frac{\partial v_i}{\partial\xi})+\frac{\partial}{\partial\eta}(J\frac{1}{r}\eta_\theta\zeta_\theta\frac{\partial v_i}{\partial\zeta})+\frac{\partial}{\partial\eta}(J\frac{1}{r}\eta_\theta\eta_\theta\frac{\partial v_i}{\partial\eta}) \\ +\ &\frac{\partial}{\partial\xi}(Jr\xi_z\xi_z\frac{\partial v_i}{\partial\xi})+\frac{\partial}{\partial\xi}(Jr\xi_z\zeta_z\frac{\partial v_i}{\partial\zeta})+\frac{\partial}{\partial\xi}(Jr\xi_z\eta_z\frac{\partial v_i}{\partial\eta}) \\ +\ &\frac{\partial}{\partial\zeta}(Jr\zeta_z\xi_z\frac{\partial v_i}{\partial\xi})+\frac{\partial}{\partial\zeta}(Jr\zeta_z\zeta_z\frac{\partial v_i}{\partial\zeta})+\frac{\partial}{\partial\zeta}(Jr\zeta_z\eta_z\frac{\partial v_i}{\partial\eta}) \\ +\ &\frac{\partial}{\partial\eta}(Jr\eta_z\xi_z\frac{\partial v_i}{\partial\xi})+\frac{\partial}{\partial\eta}(Jr\eta_z\zeta_z\frac{\partial v_i}{\partial\zeta})+\frac{\partial}{\partial\eta}(Jr\eta_z\eta_z\frac{\partial v_i}{\partial\eta}) \\ +\ &e_r\Big(-J\frac{v_r}{r}-J\frac{2}{r}\Big(\xi_\theta\frac{\partial v_\theta}{\partial\xi}+\zeta_\theta\frac{\partial v_\theta}{\partial\zeta}+\eta_\theta\frac{\partial v_\theta}{\partial\eta}\Big)\Big) \end{aligned}$$

$$+ \quad e_\theta\Big(- J\frac{v_\theta}{\theta} + J\frac{2}{r}\Big(\xi_\theta\frac{\partial v_r}{\partial \xi} + \zeta_\theta\frac{\partial v_r}{\partial \zeta} + \eta_\theta\frac{\partial v_r}{\partial \eta}\Big)\Big)\Big]$$
$$+ \quad e_z\Big(\frac{1}{r}\frac{Gr}{Re^2}T\Big), \tag{9}$$

where $v_i = (v_r, v_\theta, v_z)$.
[Energy equation]

$$\frac{\partial T}{\partial t} + (v_i \cdot \nabla)T = \frac{1}{Ma}\nabla^2 T \tag{10}$$

Equation (10) is expanded as equation (11).

$$\begin{aligned}
&\frac{\partial T}{\partial t} + \xi_t\frac{\partial T}{\partial \xi} + \zeta_t\frac{\partial T}{\partial \zeta} + \eta_t\frac{\partial T}{\partial \eta} \\
&+ \quad \frac{1}{Jr}\Big[\frac{\partial}{\partial \xi}(JrV_\xi T) + \frac{\partial}{\partial \zeta}(JrV_\zeta T) + \frac{\partial}{\partial \eta}(JrV_\eta T)\Big] \\
&= \tfrac{1}{Ma}\tfrac{1}{Jr}\Big[\ \frac{\partial}{\partial \xi}(Jr\xi_r\xi_r\frac{\partial T}{\partial \xi}) + \frac{\partial}{\partial \xi}(Jr\xi_r\zeta_r\frac{\partial T}{\partial \zeta}) + \frac{\partial}{\partial \xi}(Jr\xi_r\eta_r\frac{\partial T}{\partial \eta}) \\
&+ \quad \frac{\partial}{\partial \zeta}(Jr\zeta_r\xi_r\frac{\partial T}{\partial \xi}) + \frac{\partial}{\partial \zeta}(Jr\zeta_r\zeta_r\frac{\partial T}{\partial \zeta}) + \frac{\partial}{\partial \zeta}(Jr\zeta_r\eta_r\frac{\partial T}{\partial \eta}) \\
&+ \quad \frac{\partial}{\partial \eta}(Jr\eta_r\xi_r\frac{\partial T}{\partial \xi}) + \frac{\partial}{\partial \eta}(Jr\eta_r\zeta_r\frac{\partial T}{\partial \zeta}) + \frac{\partial}{\partial \eta}(Jr\eta_r\eta_r\frac{\partial T}{\partial \eta}) \\
&+ \quad \frac{\partial}{\partial \xi}(J\frac{1}{r}\xi_\theta\xi_\theta\frac{\partial T}{\partial \xi}) + \frac{\partial}{\partial \xi}(J\frac{1}{r}\xi_\theta\zeta_\theta\frac{\partial T}{\partial \zeta}) + \frac{\partial}{\partial \xi}(J\frac{1}{r}\xi_\theta\eta_\theta\frac{\partial T}{\partial \eta}) \\
&+ \quad \frac{\partial}{\partial \zeta}(J\frac{1}{r}\zeta_\theta\xi_\theta\frac{\partial T}{\partial \xi}) + \frac{\partial}{\partial \zeta}(J\frac{1}{r}\zeta_\theta\zeta_\theta\frac{\partial T}{\partial \zeta}) + \frac{\partial}{\partial \zeta}(J\frac{1}{r}\zeta_\theta\eta_\theta\frac{\partial T}{\partial \eta}) \\
&+ \quad \frac{\partial}{\partial \eta}(J\frac{1}{r}\eta_\theta\xi_\theta\frac{\partial T}{\partial \xi}) + \frac{\partial}{\partial \eta}(J\frac{1}{r}\eta_\theta\zeta_\theta\frac{\partial T}{\partial \zeta}) + \frac{\partial}{\partial \eta}(J\frac{1}{r}\eta_\theta\eta_\theta\frac{\partial T}{\partial \eta}) \\
&+ \quad \frac{\partial}{\partial \xi}(Jr\xi_z\xi_z\frac{\partial T}{\partial \xi}) + \frac{\partial}{\partial \xi}(Jr\xi_z\zeta_z\frac{\partial T}{\partial \zeta}) + \frac{\partial}{\partial \xi}(Jr\xi_z\eta_z\frac{\partial T}{\partial \eta}) \\
&+ \quad \frac{\partial}{\partial \zeta}(Jr\zeta_z\xi_z\frac{\partial T}{\partial \xi}) + \frac{\partial}{\partial \zeta}(Jr\zeta_z\zeta_z\frac{\partial T}{\partial \zeta}) + \frac{\partial}{\partial \zeta}(Jr\zeta_z\eta_z\frac{\partial T}{\partial \eta}) \\
&+ \quad \frac{\partial}{\partial \eta}(Jr\eta_z\xi_z\frac{\partial T}{\partial \xi}) + \frac{\partial}{\partial \eta}(Jr\eta_z\zeta_z\frac{\partial T}{\partial \zeta}) + \frac{\partial}{\partial \eta}(Jr\eta_z\eta_z\frac{\partial T}{\partial \eta})\Big]
\end{aligned} \tag{11}$$

3.2 The coupling and time advancement

In this analysis, fractional step method is utilized to computate these governing equations. Euler method is adapted for time advancement.
Here, the time in the computational domain is defined as the same time in the physical domain ($\tau = t$).
Equation (9) is described as

$$\frac{\partial v_i}{\partial \tau} + f_t + f_c = -\Big(\xi_i\frac{\partial P}{\partial \xi} + \zeta_i\frac{\partial P}{\partial \zeta} + \eta_i\frac{\partial P}{\partial \eta}\Big)e_i + f_v\,, \tag{12}$$

where f_t, f_c and f_v are the coordinate movement, convection and viscosity terms, respectively.
In fractional step method, the velocity is solved by dividing into three steps as below.

$$\tilde{v_i} = v_i^{(n)} + \Delta t \cdot \{-f_c + f_v\} \tag{13}$$

$$\hat{v_i} = \tilde{v_i} - \Delta t \cdot \left(\xi_i \frac{\partial P^{(n+1)}}{\partial \xi} + \zeta_i \frac{\partial P^{(n+1)}}{\partial \zeta} + \eta_i \frac{\partial P^{(n+1)}}{\partial \eta}\right) e_i \tag{14}$$

$$v_i^{(n+1)} = \hat{v_i} + \Delta t \cdot \{-f_t\} \tag{15}$$

Where $\tilde{v}$ means temporally velocity, and superscript (n) indicates a time step. $\hat{v_i}$ is a temporally velocity without considering the movement of the computational gird. Because the free surface deforms, the computational grid must be restructured. Therefore, it is important that the influence of the computational grid movement is considered. Equation (15) is utilized to take account of the computational grid movement.
Equation (15) is considering in two dimensional coordinate for the simplicity.
Jacobian matrix in two dimension can be described as

$$\begin{bmatrix} \frac{\partial}{\partial t} \\ \frac{\partial}{\partial r} \\ \frac{\partial}{\partial z} \end{bmatrix} = \begin{bmatrix} 1 & \xi_t & \eta_t \\ 0 & \xi_r & \eta_r \\ 0 & \xi_z & \eta_z \end{bmatrix} \begin{bmatrix} \frac{\partial}{\partial \tau} \\ \frac{\partial}{\partial \xi} \\ \frac{\partial}{\partial \eta} \end{bmatrix} \tag{16}$$

$$\begin{bmatrix} \frac{\partial}{\partial \tau} \\ \frac{\partial}{\partial \xi} \\ \frac{\partial}{\partial \eta} \end{bmatrix} = \begin{bmatrix} 1 & r_\tau & z_\tau \\ 0 & r_\xi & z_\xi \\ 0 & r_\eta & z_\eta \end{bmatrix} \begin{bmatrix} \frac{\partial}{\partial t} \\ \frac{\partial}{\partial r} \\ \frac{\partial}{\partial z} \end{bmatrix}. \tag{17}$$

Equation (17) is inversely transformed as follows,

$$\begin{bmatrix} \frac{\partial}{\partial t} \\ \frac{\partial}{\partial r} \\ \frac{\partial}{\partial z} \end{bmatrix} = \frac{1}{J} \begin{bmatrix} (r_\xi z_\eta - z_\xi r_\eta) & (-r_\tau z_\eta + z_\tau r_\eta) & (r_\tau z_\xi - r_\tau z_\xi) \\ 0 & z_\eta & -z_\xi \\ 0 & -r_\eta & r_\xi \end{bmatrix} \begin{bmatrix} \frac{\partial}{\partial \tau} \\ \frac{\partial}{\partial \xi} \\ \frac{\partial}{\partial \eta} \end{bmatrix}. \tag{18}$$

From Eqs. (16) and (18), the relation of each components are given by

$$\begin{cases} J = r_\xi z_\eta - z_\xi r_\eta \\ \xi_r = \frac{z_\eta}{J}, \qquad \eta_r = -\frac{z_\xi}{J} \\ \xi_z = -\frac{r_\eta}{J}, \qquad \eta_z = \frac{r_\xi}{J} \end{cases}. \tag{19}$$

Then equation (15) becomes equation (20) and is further transformed to equation (21).

$$v_i^{(n+1)} = \hat{v_i} - \Delta t \left[\xi_t \frac{\partial \hat{v_i}}{\partial \xi} + \eta_t \frac{\partial \hat{v_i}}{\partial \eta}\right] \tag{20}$$

$$v_i^{(n+1)} = \hat{v_i} + \Delta t \left\{\frac{\partial \hat{v_i}}{\partial r} r_t + \frac{\partial \hat{v_i}}{\partial z} z_t\right\} \tag{21}$$

Where $\hat{v_i}$ is the velocity in the previous computational grid.
That is, if the computational grid moves $\frac{\partial r}{\partial t}\Delta t$, the velocity in the restructured grid is indicated by equation (21) (See Figure. 2).
This approach can be adapted in the three dimension as well.

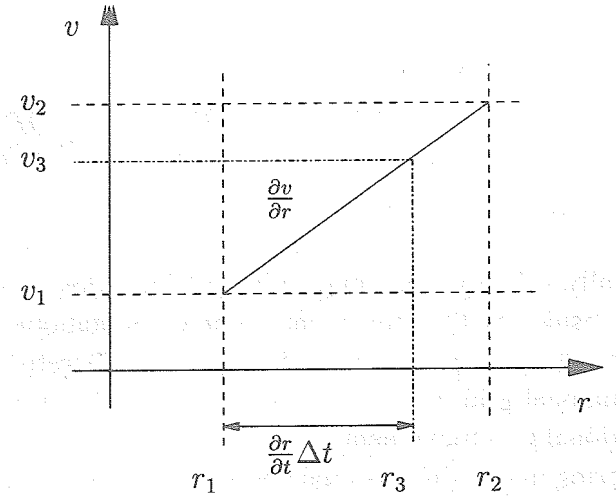

Figure 2: The relation between the velocity and the computational grid

The pressure in the equation (14) is solved by the pressure poisson equation. The pressure poisson equation is derived from the continuity equation and equation (14).
[Pressure poisson equation]

$$\nabla^2 P = \frac{\nabla \cdot v_i}{\triangle t} \tag{22}$$

Equation (22) is expanded as follows.

$$\begin{aligned}
& \frac{\partial}{\partial\xi}(Jr\xi_r\xi_r\frac{\partial P}{\partial\xi}) + \frac{\partial}{\partial\xi}(Jr\xi_r\zeta_r\frac{\partial P}{\partial\zeta}) + \frac{\partial}{\partial\xi}(Jr\xi_r\eta_r\frac{\partial P}{\partial\eta}) \\
+ & \frac{\partial}{\partial\zeta}(Jr\zeta_r\xi_r\frac{\partial P}{\partial\xi}) + \frac{\partial}{\partial\zeta}(Jr\zeta_r\zeta_r\frac{\partial P}{\partial\zeta}) + \frac{\partial}{\partial\zeta}(Jr\zeta_r\eta_r\frac{\partial P}{\partial\eta}) \\
+ & \frac{\partial}{\partial\eta}(Jr\eta_r\xi_r\frac{\partial P}{\partial\xi}) + \frac{\partial}{\partial\eta}(Jr\eta_r\zeta_r\frac{\partial P}{\partial\zeta}) + \frac{\partial}{\partial\eta}(Jr\eta_r\eta_r\frac{\partial P}{\partial\eta}) \\
+ & \frac{\partial}{\partial\xi}(J\frac{1}{r}\xi_\theta\xi_\theta\frac{\partial P}{\partial\xi}) + \frac{\partial}{\partial\xi}(J\frac{1}{r}\xi_\theta\zeta_\theta\frac{\partial P}{\partial\zeta}) + \frac{\partial}{\partial\xi}(J\frac{1}{r}\xi_\theta\eta_\theta\frac{\partial P}{\partial\eta}) \\
+ & \frac{\partial}{\partial\zeta}(J\frac{1}{r}\zeta_\theta\xi_\theta\frac{\partial P}{\partial\xi}) + \frac{\partial}{\partial\zeta}(J\frac{1}{r}\zeta_\theta\zeta_\theta\frac{\partial P}{\partial\zeta}) + \frac{\partial}{\partial\zeta}(J\frac{1}{r}\zeta_\theta\eta_\theta\frac{\partial P}{\partial\eta}) \\
+ & \frac{\partial}{\partial\eta}(J\frac{1}{r}\eta_\theta\xi_\theta\frac{\partial P}{\partial\xi}) + \frac{\partial}{\partial\eta}(J\frac{1}{r}\eta_\theta\zeta_\theta\frac{\partial P}{\partial\zeta}) + \frac{\partial}{\partial\eta}(J\frac{1}{r}\eta_\theta\eta_\theta\frac{\partial P}{\partial\eta}) \\
+ & \frac{\partial}{\partial\xi}(Jr\xi_z\xi_z\frac{\partial P}{\partial\xi}) + \frac{\partial}{\partial\xi}(Jr\xi_z\zeta_z\frac{\partial P}{\partial\zeta}) + \frac{\partial}{\partial\xi}(Jr\xi_z\eta_z\frac{\partial P}{\partial\eta}) \\
+ & \frac{\partial}{\partial\zeta}(Jr\zeta_z\xi_z\frac{\partial P}{\partial\xi}) + \frac{\partial}{\partial\zeta}(Jr\zeta_z\zeta_z\frac{\partial P}{\partial\zeta}) + \frac{\partial}{\partial\zeta}(Jr\zeta_z\eta_z\frac{\partial P}{\partial\eta}) \\
+ & \frac{\partial}{\partial\eta}(Jr\eta_z\xi_z\frac{\partial P}{\partial\xi}) + \frac{\partial}{\partial\eta}(Jr\eta_z\zeta_z\frac{\partial P}{\partial\zeta}) + \frac{\partial}{\partial\eta}(Jr\eta_z\eta_z\frac{\partial P}{\partial\eta}) \\
= & \frac{1}{\triangle t}\Big[\frac{\partial}{\partial\xi}(Jr\tilde{V_\xi}) + \frac{\partial}{\partial\zeta}(Jr\tilde{V_\zeta}) + \frac{\partial}{\partial\eta}(Jr\tilde{V_\eta})\Big]
\end{aligned} \tag{23}$$

Where $\tilde{V_\xi}$,$\tilde{V_\zeta}$ and $\tilde{V_\eta}$ are defined by

$$\tilde{V_\xi} = \xi_r\tilde{v_r} + \frac{1}{r}\xi_\theta\tilde{v_\theta} + \xi_z\tilde{v_z}$$

$$\tilde{V_\zeta} = \zeta_r \tilde{v_r} + \frac{1}{r}\zeta_\theta \tilde{v_\theta} + \zeta_z \tilde{v_z}$$
$$\tilde{V_\eta} = \eta_r \tilde{v_r} + \frac{1}{r}\eta_\theta \tilde{v_\theta} + \eta_z \tilde{v_z} \ ,$$

which are called as **contravariant temporally velocities.**
To solve the pressure variation implicitly, equation (23) is calculated by successive over relaxation method (SOR method) in this analysis.

3.3 Boundary condition

3.3.1 Boundary condition of the velocity

To derive the boundary condition of the velocity at the free surface, the balance between the shearing stress and the surface tension must be considered.
The relation between the shearing stress and the surface tension is shown in figure 3.

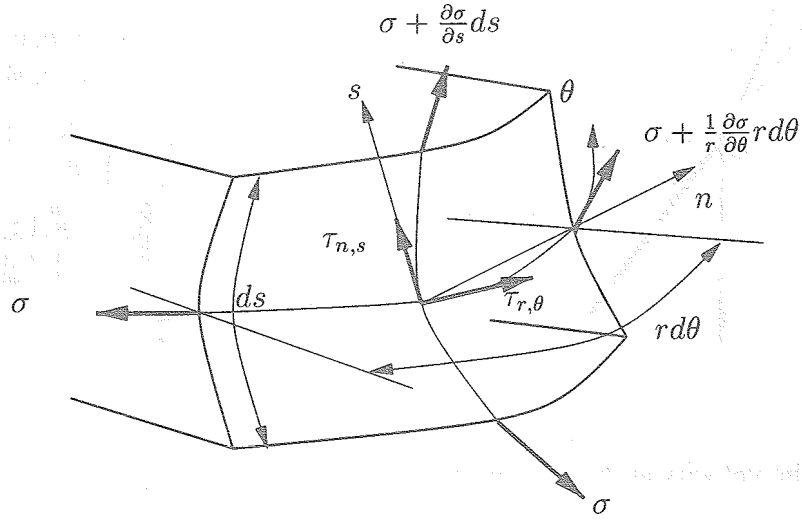

Figure 3: The stress balance between the shearing stress and the surface tension

From figure 3, the equations of the balance between shearing stress and the surface tension are described as

$$\begin{cases} \tau_{n,s} \cdot r d\theta ds = \{(\sigma + \frac{\partial \sigma}{\partial s} \cdot ds) - \sigma\} \cdot r d\theta \\ \tau_{r,\theta} \cdot r d\theta ds = \{(\sigma + \frac{1}{r}\frac{\partial \sigma}{\partial \theta} \cdot r d\theta) - \sigma\} \cdot ds \end{cases} \tag{24}$$

Newton's law of viscosity equation is expressed as follows.

$$\begin{cases} \tau_{n,s} = \mu\{\frac{\partial v_s}{\partial n} + \frac{\partial v_n}{\partial s}\} \\ \tau_{r,\theta} = \mu\{\frac{1}{r}\frac{\partial v_r}{\partial \theta} + r\frac{\partial}{\partial r}(\frac{v_\theta}{r})\} \end{cases} \tag{25}$$

From Eqs. (24) and (25) equation (26) is derived.

$$\begin{cases} \mu\{\frac{\partial v_s}{\partial n} + \frac{\partial v_n}{\partial s}\} = \frac{\partial \sigma}{\partial s} \\ \mu\{\frac{1}{r}\frac{\partial v_r}{\partial \theta} + r\frac{\partial}{\partial r}(\frac{v_\theta}{r})\} = \frac{1}{r}\frac{\partial \sigma}{\partial \theta} \end{cases} \tag{26}$$

If the velocity upon the free surface in the normal direction is assumed to be zero, equation (26) can be shown as follows.

$$\begin{cases} \mu\frac{\partial v_s}{\partial n} = \frac{\partial \sigma}{\partial s} \\ \mu\{\frac{1}{r}\frac{\partial v_r}{\partial \theta} + r\frac{\partial}{\partial r}(\frac{v_\theta}{r})\} = \frac{1}{r}\frac{\partial \sigma}{\partial \theta} \end{cases} \tag{27}$$

Equation (27) can be non-dimensionalized as following equations.

$$\begin{cases} \frac{\partial v_s}{\partial n} = -\frac{\partial T}{\partial s} \\ \frac{1}{r}\frac{\partial v_r}{\partial \theta} + r\frac{\partial}{\partial r}(\frac{v_\theta}{r}) = -\frac{1}{r}\frac{\partial T}{\partial \theta} \end{cases} \tag{28}$$

In the equation of the relation between normal and tangential directions, the tangential velocity v_s is divided into radius and axial directions (See figure. 4).

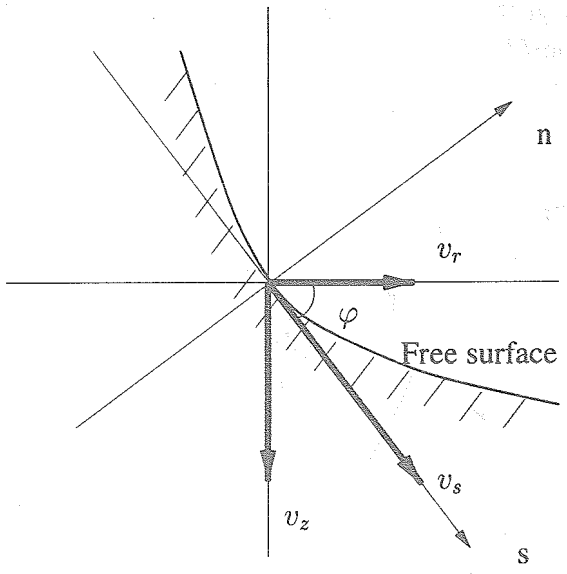

$$\begin{cases} v_r = v_s\cos\varphi \\ v_z = v_s\sin\varphi \end{cases} \tag{29}$$

$$\Longleftrightarrow \begin{cases} v_s = \frac{v_r}{\cos\varphi} \\ v_s = \frac{v_z}{\sin\varphi} \end{cases} \tag{30}$$

$$\Longleftrightarrow \begin{cases} \frac{\partial v_s}{\partial n} = \frac{\partial}{\partial n}(\frac{v_r}{\cos\varphi}) \\ \frac{\partial v_s}{\partial n} = \frac{\partial}{\partial n}(\frac{v_z}{\sin\varphi}) \end{cases} \tag{31}$$

$$\Longleftrightarrow \begin{cases} \frac{\partial v_r}{\partial n} = -\cos\varphi\frac{\partial T}{\partial s} \\ \frac{\partial v_z}{\partial n} = -\sin\varphi\frac{\partial T}{\partial s} \end{cases} \tag{32}$$

Figure 4: The velocity at the free surface

Generally the following relations are derived in the normal and tangential directions.
[Normal derivatives]

$$\frac{\partial \phi}{\partial n^{(\xi)}} = \frac{1}{J\sqrt{\alpha}}(\alpha\phi_\xi - \beta\phi_\eta) \tag{33}$$

$$\frac{\partial \phi}{\partial n^{(\eta)}} = \frac{1}{J\sqrt{\gamma}}(-\beta\phi_\xi + \gamma\phi_\eta) \tag{34}$$

[Tangential derivatives]

$$\frac{\partial \phi}{\partial s^{(\xi)}} = \frac{1}{\sqrt{\alpha}}\phi_\eta \tag{35}$$

$$\frac{\partial \phi}{\partial s^{(\eta)}} = \frac{1}{\sqrt{\gamma}}\phi_\xi \tag{36}$$

Here $\alpha = r_\eta^2 + z_\eta^2, \quad \beta = r_\xi r_\eta + z_\xi z_\eta, \quad \gamma = r_\xi^2 + z_\xi^2$.
Using equation (33), the equation of the stress balance between normal and tangential directions is obtained.

$$\frac{1}{J\sqrt{\alpha}}(\alpha\frac{\partial v_z}{\partial \xi} - \beta\frac{\partial v_z}{\partial \eta}) = -\sin\varphi\frac{1}{\sqrt{\alpha}}\frac{\partial T}{\partial \eta} \tag{37}$$

The axial velocity v_z is derived from equation (37). And the radius velocity is derived from the relation of following equation.

$$v_r = \frac{\cos\varphi}{\sin\varphi} v_z \tag{38}$$

On the other hand, the boundary condition of the circumferential velocity is defined by

$$\frac{1}{r}\frac{\partial v_r}{\partial \theta} + r\frac{\partial}{\partial r}\left(\frac{v_\theta}{r}\right) = -\frac{1}{r}\frac{\partial T}{\partial \theta} \tag{39}$$

Equation (39) is transformed to the computational domain by the Jacobian matrix as

$$\begin{aligned} &\frac{1}{r}\left\{\xi_\theta\frac{\partial v_r}{\partial \xi} + \zeta_\theta\frac{\partial v_r}{\partial \zeta} + \eta_\theta\frac{\partial v_r}{\partial \eta}\right\} + r\left\{\xi_r\frac{\partial}{\partial \xi}\left(\frac{v_\theta}{r}\right) + \zeta_r\frac{\partial}{\partial \zeta}\left(\frac{v_\theta}{r}\right) + \eta_r\frac{\partial}{\partial \eta}\left(\frac{v_\theta}{r}\right)\right\} \\ = \; &-\frac{1}{r}\left\{\xi_\theta\frac{\partial T}{\partial \xi} + \zeta_\theta\frac{\partial T}{\partial \zeta} + \eta_\theta\frac{\partial T}{\partial \eta}\right\} . \end{aligned} \tag{40}$$

3.3.2 Boundary condition of the temperature

The condition of the heat transfer over the free surface is assumed to be adiabatic. Therefore the equation of the boundary condition of the temperature is

$$\frac{\partial T}{\partial n} = 0 \tag{41}$$

Equation (41) is transformed by the Jacobian matrix as

$$\frac{\partial T}{\partial \xi}\frac{\partial \xi}{\partial n} + \frac{\partial T}{\partial \zeta}\frac{\partial \zeta}{\partial n} + \frac{\partial T}{\partial \eta}\frac{\partial \eta}{\partial n} = 0 . \tag{42}$$

To transform into the computational domain, equation (33) is utilized.

$$\frac{\partial T}{\partial n} = \frac{1}{J\sqrt{\alpha}}\left(\alpha\frac{\partial T}{\partial \xi} - \beta\frac{\partial T}{\partial \eta}\right) = 0 \tag{43}$$

3.3.3 The treatment of the liquid center axis

In this analysis the governing equations are described in the cylindrical coordinate. Therefore the center of the cylinder ($r = 0$) can not be solved directly by the present equations (Eqs.(2)-(3)). This problem is solved through by the method below. The computational grid is fixed at the center.

[Navier-Stokes equation of the liquid center (axial direction)]

$$\begin{aligned} &r\frac{\partial v_z}{\partial t} + \frac{\partial}{\partial r}(r v_r v_z) + \frac{\partial}{\partial \theta}(v_\theta v_z) + \frac{\partial}{\partial z}(r v_z^2) \\ = \; &-r\frac{\partial P}{\partial z} + \frac{Pr}{Ma}\left[\frac{\partial}{\partial r}\left(r\frac{\partial v_z}{\partial r}\right) + \frac{\partial}{\partial \theta}\left(\frac{1}{r}\frac{\partial v_z}{\partial \theta}\right) + \frac{\partial}{\partial z}\left(r\frac{\partial v_z}{\partial z}\right)\right] + rT\frac{Gr}{Re^2} \end{aligned} \tag{44}$$

Equation (44) is integrated in all directions.

$$\frac{\partial v_z}{\partial t} + \frac{\Delta\theta}{\pi\Delta r}\sum_{\theta=0}^{2\pi}(v_r v_z) + \frac{1}{\Delta z}\left[v_z^2\right]_0^{\Delta z}$$
$$= -\frac{\partial P}{\partial z} + \frac{Pr}{Ma}\left[\frac{\Delta\theta}{\pi\Delta r}\sum_{\theta=0}^{2\pi}\frac{\partial v_z}{\partial r}\Big|_{\Delta r} + \frac{1}{\Delta z}\left[\frac{\partial v_z}{\partial z}\right]_0^{\Delta z}\right] + \frac{Gr}{Re^2}T \tag{45}$$

As for the radius and circumference velocity in the center, the velocity is summed over the surrounding mesh points (See figure 5).

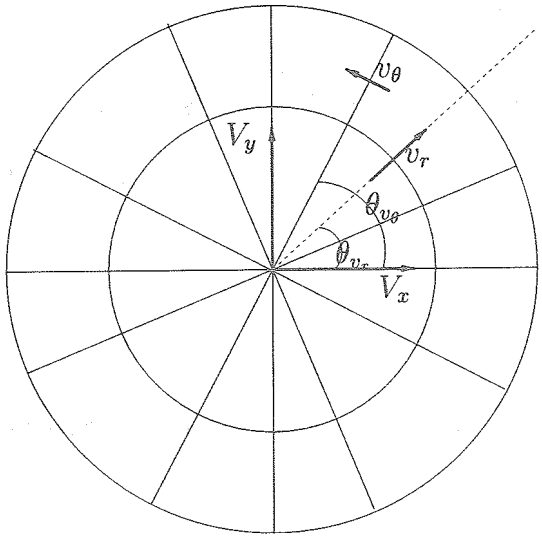

$$V_x = \sum_{j=0}^{2\pi}\left\{v_r\cos\theta_{v_r} + v_\theta\cos(\theta_{v_\theta}+\frac{\pi}{2})\right\} \tag{46}$$

$$V_y = \sum_{j=0}^{2\pi}\left\{v_r\sin\theta_{v_r} + v_\theta\sin(\theta_{v_\theta}+\frac{\pi}{2})\right\} \tag{47}$$

Figure 5: The velocity at the center axis

After the summation, the velocities V_x, V_y are divided into the radius and circumference components (v_r, v_θ).

$$v_r = \left[V_x\cos\theta_{v_r} + V_y\cos(\frac{\pi}{2}-\theta_{v_r})\right]\frac{1}{nj} \tag{48}$$

$$v_\theta = \left[V_x(-\sin\theta_{v_\theta}) + V_y\sin(\frac{\pi}{2}-\theta_{v_\theta})\right]\frac{1}{nj} \tag{49}$$

Here nj shows the division number of the circumference direction. Such treatment at the center axis is also applied to the energy equation.
[Energy equation of the liquid center]

$$r\frac{\partial T}{\partial t} + \frac{\partial}{\partial r}(rv_rT) + \frac{\partial}{\partial\theta}(v_\theta T) + \frac{\partial}{\partial z}(rv_zT) = \frac{1}{Ma}\left[\frac{\partial}{\partial r}(r\frac{\partial T}{\partial r}) + \frac{\partial}{\partial\theta}(\frac{1}{r}\frac{\partial T}{\partial\theta}) + \frac{\partial}{\partial z}(r\frac{\partial T}{\partial z})\right] \tag{50}$$

Equation (50) is integrated in all directions.

$$\frac{\partial T}{\partial t} + \frac{\Delta\theta}{\pi\Delta r}\sum_{\theta=0}^{2\pi}(v_rT) + \frac{1}{\Delta z}\left[v_zT\right]_0^{\Delta z} = \frac{1}{Ma}\left\{\frac{\Delta\theta}{\pi\Delta r}\sum_{\theta=0}^{2\pi}\frac{\partial T}{\partial r}\Big|_{\Delta r} + \frac{1}{\Delta z}\left[\frac{\partial T}{\partial z}\right]_0^{\Delta z}\right\} \tag{51}$$

Also the pressure Poisson equation has to be solved at the liquid center axis.

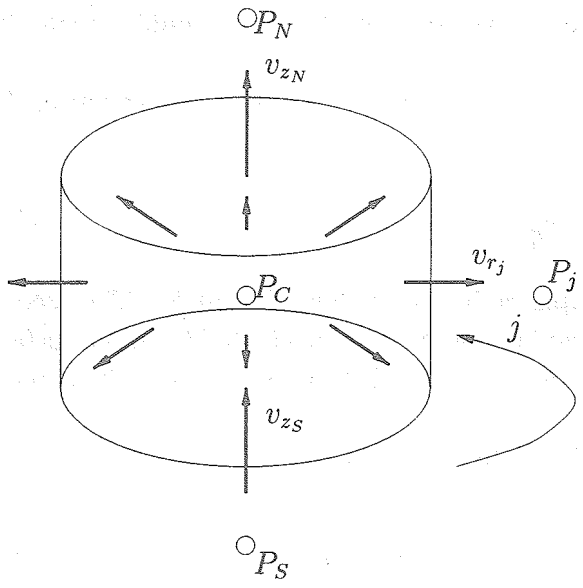

Figure 6: The model of the in and outflows

From the figure 6 the continuity equation is defined as

$$\pi\Delta r^2(v_{z_N} - v_{z_S}) + \frac{2\pi}{nj}\Delta r\Delta z\sum_{j=0}^{nj} v_{r_j} = 0. \quad (52)$$

Time advancement is described as follows.

$$\begin{cases} v_{z_N}^{(n+1)} = \tilde{v}_{z_N} - \Delta t\frac{P_N - P_C}{\Delta z} \\ v_{z_S}^{(n+1)} = \tilde{v}_{z_S} - \Delta t\frac{P_C - P_S}{\Delta z} \\ v_{r_j}^{(n+1)} = \tilde{v}_{r_j} - \Delta t\frac{P_j - P_C}{\Delta r + \frac{1}{2}\Delta r_j} \end{cases} \quad (53)$$

where, Δr_j is defined as $\Delta r_j = \Delta r$.

The pressure Poisson equation is derived from Eqs. (52) and (53).

$$\left[\frac{2}{\Delta z^2} + \frac{4}{3\Delta r^2}\right] P_C - \left[\frac{1}{\Delta z^2}(P_N + P_S) + \frac{1}{nj}\frac{4}{3\Delta r^2}\sum_{j=0}^{nj} P_j\right]$$
$$= \left[-\frac{1}{\Delta z}(\tilde{v}_{z_N} - \tilde{v}_{z_S}) - \frac{2}{nj\Delta r}\sum_{j=0}^{nj}\tilde{v}_{r_j}\right]\frac{1}{\Delta t} \quad (54)$$

3.4 The free surface shape

To computate the free surface shape, the stress balance over the free surface must be considered. Along the free surface between two immiscible fluids (1) and (2) the forces on adjacent surface element of (1) and (2) must be the same.
If the surface is plane and the surface tension is constant, the stress balance over the free surface leads

$$\mathbb{S}^{(1)} \cdot \mathbf{n} = \mathbb{S}^{(2)} \cdot \mathbf{n}, \quad (55)$$

where $\mathbb{S}$ is the stress tensor.
The each components in the stress tensor are described as

$$S_{ij} = -P\delta_{ij} + \lambda\Theta\delta_{ij} + \mu e_{ij}, \quad (56)$$

where λ and μ are **coefficient of viscosity** and **second coefficient of viscosity**, respectively.
In this analysis it is assumed that the fluid is Newtonian, so that

$$\Theta = div\nu = 0. \quad (57)$$

In addition, if the free surface has curvature and the surface tension varies along the interface, the equation of the stress balance is described as [5]

$$\mathbb{S}^{(1)} \cdot \mathbf{n} + \sigma(\nabla \cdot \mathbf{n})\mathbf{n} - (\mathbf{I} - \mathbf{nn}) \cdot \nabla\sigma = \mathbb{S}^{(2)} \cdot \mathbf{n}, \quad (58)$$

where $\mathbb{I}$ is the identity matrix, and $\mathbf{n}$ is the unit normal vector directed out of liquid (1) into the ambient fluid (2).
The element $\sigma(\nabla \cdot \mathbf{n})$ in the second term is the Laplace pressure. The mean curvature of the interface,

$$\nabla \cdot \mathbf{n} = \frac{1}{R_1} + \frac{1}{R_2}, \tag{59}$$

can be expressed as the sum of the inverse principle radii of curvature R_1 and R_2. The second term in equation (58) indicates the surface force acting tangentially originated from the surface tension σ. The operator $\mathbb{I} - \mathbf{nn}$ represents the orthogonal projection of a vector onto the tangent plane defined by $\mathbf{n}$.
Besides the influence of the surface shape and the surface tension, the action of the gravity is taken account into the equation of the stress balance,

$$\mathbb{S}^{(1)} \cdot \mathbf{n} + \sigma(\nabla \cdot \mathbf{n})\mathbf{n} - (\mathbb{I} - \mathbf{nn}) \cdot \nabla\sigma + \rho^{(1)} g(H - z)\mathbf{n} = \mathbb{S}^{(2)} \cdot \mathbf{n} + \rho^{(2)} g(H - z)\mathbf{n} \tag{60}$$

Equation (60) is described in non-dimensional manner.

$$\mathbb{S}^{(1)} \cdot \mathbf{n} + \left(\frac{1}{Ca} - T^*\right)(\nabla \cdot \mathbf{n})\mathbf{n} + (\mathbb{I} - \mathbf{nn}) \cdot \nabla T^* = \mathbb{S}^{(2)} - \frac{Bo}{Ca}(H - z)\mathbf{n} \tag{61}$$

The scales used for non-dimensionalization were indicated in table 1. In addition, the normalized temperature $T^* = (T - T_0)/\Delta T$ has been introduced.
The surface tension is non-dimensionalized by using the normalized temperature,

$$\sigma(T) = \sigma_0(T_0) - \sigma_T(T - T_0) \tag{62}$$

$$\Longleftrightarrow \frac{\sigma}{\sigma_T \Delta T} = \frac{\sigma_0(T_0)}{\sigma_T \Delta T} - T^* \tag{63}$$

$$\Longleftrightarrow \sigma^* = \frac{1}{Ca} - T^*, \tag{64}$$

where $\sigma^* = \frac{\sigma}{\sigma_T \Delta T}$ and the capillary number is defined by

$$Ca = \frac{\sigma_T \Delta T}{\sigma_0(T_0)}. \tag{65}$$

From equation (64), the gradient of the surface tension is expressed by the normalized temperature,

$$\nabla\sigma^* = -\nabla T^*. \tag{66}$$

Bo is called as **Bond number** which is defined by

$$Bo = \frac{(\rho^{(1)} - \rho^{(2)})gH^2}{\sigma_0}. \tag{67}$$

The asterisk is omitted hereafter.
Equation (61) is expanded as follows.
Using the unit normal vector

$$\mathbf{n} = \frac{1}{N}\left(\mathbf{e}_r - \frac{1}{R}\frac{\partial R}{\partial \theta}\mathbf{e}_\theta - \frac{\partial R}{\partial z}\mathbf{e}_z\right) \tag{68}$$

with the normalizing denominator

$$N = \left[1 + \left(\frac{\partial R}{\partial z}\right)^2 + \frac{1}{R^2}\left(\frac{\partial R}{\partial \theta}\right)^2\right]^{\frac{1}{2}}, \tag{69}$$

the surface curvature can be expressed as

$$\begin{aligned}\nabla \cdot \mathbf{n} = \frac{-1}{R^3 N^3}\Bigg[& R\frac{\partial^2 R}{\partial z^2}\left\{R^2 + \left(\frac{\partial R}{\partial \theta}\right)^2\right\} \\ & + 2\frac{\partial R}{\partial z}\frac{\partial R}{\partial \theta}\left(\frac{\partial R}{\partial z}\frac{\partial R}{\partial \theta} - R\frac{\partial^2 R}{\partial z \partial \theta}\right) \\ & - \left\{1 + \left(\frac{\partial R}{\partial z}\right)^2\right\}\left\{R^2 + 2\left(\frac{\partial R}{\partial \theta}\right)^2 - R\frac{\partial^2 R}{\partial \theta^2}\right\}\Bigg].\end{aligned} \tag{70}$$

The stress tensor is indicated as

$$S_{ij} = -P\delta_{ij} + \mu e_{ij}, \tag{71}$$

where e_{ij} in the cylindrical coordinate is defined by

$$\begin{aligned} & e_{rr} = \frac{\partial v_r}{\partial r}, \quad e_{\theta\theta} = \frac{1}{r}\frac{\partial v_\theta}{\partial \theta} + \frac{v_r}{r}, \quad e_{zz} = \frac{\partial v_z}{\partial z}, \\ & e_{r\theta} = \frac{1}{2}\left\{r\frac{\partial}{\partial r}\left(\frac{v_\theta}{r}\right) + \frac{1}{r}\frac{\partial v_r}{\partial \theta}\right\}, \quad e_{\theta z} = \frac{1}{2}\left\{\frac{1}{r}\frac{\partial v_z}{\partial \theta} + \frac{\partial v_\theta}{\partial z}\right\}, \quad e_{zr} = \frac{1}{2}\left\{\frac{\partial v_r}{\partial z} + \frac{\partial v_z}{\partial r}\right\}\end{aligned} \tag{72}$$

The unit normal vector and the identity matrix are shown below.

$$\mathbf{n} = \begin{bmatrix} n_r \\ n_\theta \\ n_z \end{bmatrix} \tag{73}$$

$$\mathbf{I} = \begin{bmatrix} 1 & 0 & 0 \\ 0 & 1 & 0 \\ 0 & 0 & 1 \end{bmatrix} \tag{74}$$

$\mathbf{nn}$ represents the dyadic product which is expressed as

$$\mathbf{I} = \begin{bmatrix} n_r \\ n_\theta \\ n_z \end{bmatrix}\begin{bmatrix} n_r \\ n_\theta \\ n_z \end{bmatrix} = \begin{bmatrix} n_r^2 & n_r n_\theta & n_r n_z \\ n_\theta n_r & n_\theta^2 & n_\theta n_z \\ n_z n_r & n_z n_\theta & n_z^2 \end{bmatrix}. \tag{75}$$

The components of the surface tension gradient is

$$\nabla\sigma = \begin{bmatrix} \frac{\partial \sigma}{\partial r} \\ \frac{1}{r}\frac{\partial \sigma}{\partial \theta} \\ \frac{\partial \sigma}{\partial z} \end{bmatrix}. \tag{76}$$

From these matrices, the equation of the stress balance is led in the three directions.
Since the two directions of the curvature exist in the three dimension, the two tri-diagonal matrices must be considered for axial and circumferential directions. The tridiagonal equations

are indicated below.
(Radius direction)

$$\frac{\partial^2 R}{\partial z^2} = \frac{-R^3 N^3}{R\{R^2+(\partial R/\partial\theta)^2\}(1/Ca-T)} \left[Re(P^{(1)}-P^{(2)}) - \frac{Bo}{Ca}(H-z) - \frac{\partial v_r}{\partial r} - \frac{1}{2}\{r\frac{\partial}{\partial r}(\frac{v_\theta}{r}) + \frac{1}{r}\frac{\partial v_r}{\partial \theta}\}\frac{n_\theta}{n_r} - \frac{1}{2}\{\frac{\partial v_r}{\partial z}+\frac{\partial v_z}{\partial r}\}\frac{n_z}{n_r} - \frac{1-n_r^2}{n_r}\frac{\partial T}{\partial r} + n_\theta\frac{1}{r}\frac{\partial T}{\partial\theta} + n_z\frac{\partial T}{\partial z}\right] + \frac{1}{R\{R^2+(\partial R/\partial\theta)^2}\left[-2\frac{\partial R}{\partial z}\frac{\partial R}{\partial\theta}(\frac{\partial R}{\partial z}\frac{\partial R}{\partial\theta} - R\frac{\partial^2 R}{\partial z\partial\theta}) + \{1+(\frac{\partial R}{\partial z})^2\}\{R^2+2(\frac{\partial R}{\partial\theta})^2 - R\frac{\partial^2 R}{\partial\theta^2}\}\right] \quad (77)$$

(Circumferential direction)

$$\frac{\partial^2 R}{\partial \theta^2} = \frac{-R^3 N^3}{R\{1+(\partial R/\partial z)^2\}(1/Ca-T)} \left[Re(P^{(1)}-P^{(2)}) - \frac{Bo}{Ca}(H-z) - \frac{\partial v_r}{\partial r} - \frac{1}{2}\{r\frac{\partial}{\partial r}(\frac{v_\theta}{r}) + \frac{1}{r}\frac{\partial v_r}{\partial \theta}\}\frac{n_\theta}{n_r} - \frac{1}{2}\{\frac{\partial v_r}{\partial z}+\frac{\partial v_z}{\partial r}\}\frac{n_z}{n_r} - \frac{1-n_r^2}{n_r}\frac{\partial T}{\partial r} + n_\theta\frac{1}{r}\frac{\partial T}{\partial\theta} + n_z\frac{\partial T}{\partial z}\right] + \frac{1}{R\{1+(\partial R/\partial z)^2\}}\left[-R\frac{\partial^2 R}{\partial z^2}\{R^2+(\frac{\partial R}{\partial\theta})^2\} - 2\frac{\partial R}{\partial z}\frac{\partial R}{\partial\theta}(\frac{\partial R}{\partial z}\frac{\partial R}{\partial\theta} - R\frac{\partial^2 R}{\partial z\partial\theta})\right] + \frac{2}{R}(\frac{\partial R}{\partial\theta})^2 + R \quad (78)$$

In addition to the these tridiagonal equations, the constant volume equation has to be solved to maintain the volume of the liquid bridge.

$$\int_0^H\int_0^{2\pi}\frac{1}{2}R^2 d\theta dz = V \quad (79)$$

The position of the free surface ,R, is solved by using Tri-Diagonal Matrix Algorithm (TDMA) derived from Eqs. (61) and (79). The tri-diagonal matrices are given below.

(Axial direction)

$$
\begin{bmatrix}
a^H_{1,0} & c^H_{1,0} & & & & & & & & & & d^H_{1,0} \\
b^H_{1,1} & a^H_{1,1} & c^H_{1,1} & & & & & & & & & d^H_{1,1} \\
& & \ddots & & & & & & & & & \vdots \\
& & b^H_{1,nk} & a^H_{1,nk} & c^H_{1,nk} & & & & & & & d^H_{1,nk} \\
& & & b^H_{1,nk+1} & a^H_{1,nk+1} & & & & & & & d^H_{1,nk+1} \\
& & & & & \ddots & & & & & & \vdots \\
& & & & & & a^H_{nj,0} & c^H_{nj,0} & & & & d^H_{nj,0} \\
& & & & & & b^H_{nj,1} & a^H_{nj,1} & c^H_{nj,1} & & & d^H_{nj,1} \\
& & & & & & & & \ddots & & & \vdots \\
& & & & & & & & b^H_{nj,nk} & a^H_{nj,nk} & c^H_{nj,nk} & d^H_{nj,nk} \\
& & & & & & & & & b^H_{nj,nk+1} & a^H_{nj,nk+1} & d^H_{nj,nk+1} \\
e^H_{1,0} & e^H_{1,1} & e^H_{1,2} \cdots e^H_{1,nk-1} & e^H_{1,nk} & e^H_{1,nk+1} \cdots & e^H_{nj,0} & e^H_{nj,1} & e^H_{nj,2} \cdots & e^H_{nj,nk-1} & e^H_{nj,nk} & e^H_{nj,nk+1} & G^H
\end{bmatrix}
\begin{bmatrix}
R_{1,0} \\ R_{1,1} \\ \vdots \\ R_{1,nk} \\ R_{1,nk+1} \\ \vdots \\ R_{nj,0} \\ R_{nj,1} \\ \vdots \\ R_{nj,nk} \\ R_{nj,nk+1} \\ P_s
\end{bmatrix}
=
\begin{bmatrix}
f^H_{1,0} \\ f^H_{1,1} \\ \vdots \\ f^H_{1,nk} \\ f^H_{1,nk+1} \\ \vdots \\ f^H_{nj,0} \\ f^H_{nj,1} \\ \vdots \\ f^H_{nj,nk} \\ f^H_{nj,nk+1} \\ Q^H
\end{bmatrix}
\tag{80}
$$

The last array in this matrix gives the constant volume condition.
(Circumferential direction; for each R_k)

$$
\begin{bmatrix}
b^C_{1,k} & c^C_{1,k} & & & & a^C_{1,k} \\
a^C_{2,k} & b^C_{2,k} & c^C_{2,k} & & & \\
& & \ddots & & & \\
& & & a^C_{nj-1,k} & b^C_{nj-1,k} & c^C_{nj-1,k} \\
c^C_{nj,k} & & & & a^C_{nj,k} & b^C_{nj,k}
\end{bmatrix}
\begin{bmatrix}
R_{1,k} \\ R_{2,k} \\ \vdots \\ R_{nj-1,k} \\ R_{nj,k}
\end{bmatrix}
=
\begin{bmatrix}
d^C_{1,k} \\ d^C_{2.k} \\ \vdots \\ d^C_{nj-1,k} \\ d^C_{nj,k}
\end{bmatrix}
\tag{81}
$$

The free surface shape is derived from these matrices. However the momentum equation cannot be considered by these matrices only. Therefore the momentum equation must be included into the algorithm of the solving the free surface shape. Since the order of the free surface deformation is so small (an order of the 10^{-6} of the radius), the direction of the surface-normal can be approximated as that of the radius. The following equation is adapted to consider the time-dependent radius variation.

$$
R^{new} = R^{old} + \frac{1}{2}\Delta t(v_r^{new} + v_r^{old}) \tag{82}
$$

The free surface shape can be computated from Eqs. (80)- (82).

4 NUMERICAL ANALYSIS

4.1 Two dimensional calculation on high Prandtl number fluid

As the first step, the 2-D thermocapillary flow is calculated in a liquid bridge. Table 2 indicates the computational condition of two-dimensional calculations.

Table 2: The computational condition

	Aspect ratio (H/D)	Ma	Ca	Pr	Bo	Gr
CASE-1	0.5	28500	0.08	28	0	0
CASE-2	0.5	57000	0.08	28	0	0
CASE-3	0.5	280000	0.08	28	0	0
CASE-4	0.7	280000	0.1	28	0	0
CASE-5	0.6	27000	0.06	28	0	0
CASE-6	0.6	27000	0.06	28	4.2	1300
CASE-7	0.7	100000	0.1	28	2.0	2800
CASE-8	0.7	200000	0.1	28	0.2	5600

Figs. 7, 8 and 9 indicate the displacement of the free surface until the velocity fluctuation at the surface reaches the lower disk. The surface displacements up to the steady flow are shown in Figs. 10, 11 and 12. Figure 13 describes the free surface deformation at the steady state.
The factors affecting the difference in the surface deformation as shown in figure 13 are investigated. The each term of the equation (77) can be expressed as

$$\begin{aligned} \frac{\partial^2 R}{\partial z^2} &= (\textit{Pressure term}) + (\textit{Gravity term}) \\ &+ (\textit{Normal stress term}) + (\textit{Shearing stress term}) \\ &+ (\textit{Thermocapillary force term}) + (\textit{rest of Laplace pressure term}) , \end{aligned} \tag{83}$$

where sum of the rest of Laplace pressure and $\frac{\partial^2 R}{\partial z^2}$ corresponds to the Laplace pressure. The each term in the case of CASE-1, 2 and 3 is plotted in Figs. 14, 15 and 16, respectively. From these figures, it is known that the most dominant term on the free surface deformation is the pressure term. To observe the effect of the pressure term, the time variation of this term is plotted in figure 17. Figure 17 indicates that there is a significant difference of pressure variation between CASE-1, 2 and 3. In the case of a higher Marangoni number, an abrupt pressure drop takes place at point A in figure 13 at around time=100. Figs. 18, 19 and 20 indicate variations of the temperature, radial velocity and axial velocity at point A, respectively. The peak of the axial velocity in figure 20 corresponds to the peak of the pressure in figure 17.
The thermocapillary convection exhibits oscillatory flow in CASE-3. Figure 22 indicates the variation of the free surface temperature at the three points as shown in figure 21. The free surface temperature rises up with oscillation. The variation of the axial velocity on the free surface during the same time interval as in figure 18 are given in Figs. 23, 24 and 25. These figures indicate that the axial velocity oscillates as well as the temperature does. The amplitude of the axial velocity oscillation on the Point-3 is the largest among the three plotted points.
The variations of radial velocities are represented in figure 26. It is noted that the phase difference in radial velocity profiles exists at various heights. The vibration may propagate from upper disk to lower one.
The variations of the free surface are shown in Figs. 27, 28 and 29. These figures indicate that the free surface vibrates with surface temperature and velocity oscillation with the same period. However, the phase of the free surface vibration differs from those of the temperature and velocity vibration.

Figs. 30-34 indicate variations of the surface temperature, radial velocity, axial velocity, free surface deformation and the amplitude of the free surface under the condition of CASE-4. The oscillation occurs in this case also. The surface velocity oscillates as well as the temperature in Figs. 30-32. The amplitude of the velocity on the Point-3 is the largest among the three plotted

points. The free surface also oscillates in this time. From the figure 33, the oscillation amplitude of the free surface deformation is plotted in figure 34. Figure 34 shows that the amplitude is the largest at point-3.

Figs. 35-37 indicate the variation of the free surface deformation, surface temperature, radial velocity and axial velocity, respectively (CASE-5 and 6). The solid and dotted lines show the results under the zero-gravity and the normal gravity, respectively. The free surface deformation under the normal gravity is larger than the one under the zero-gravity. On the other hand, the axial velocity in the case under the normal gravity is smaller than the one under the zero-gravity. In these cases, the oscillation is not observed. Therefore the case of a higher Marangoni number has been simulated.

Figs. 39-42 indicate the variations of the surface temperature, surface deformation, radial velocity and axial velocity, respectively under the condition of CASE-7. In this case, the oscillation begun from about time= 1000. The free surface oscillates together with the surface temperature and velocity with the same period in these figures.

Figs. 43-45 represent a close up view of the surface temperature and velocities. Figure 46 shows the amplitude of the free surface. The amplitude of the temperature and velocities are almost the same among the three plotted points. But the amplitude of the free surface deformation in the point-2 is extremely smaller than the ones at the point-1 and 3.

Figs. 47-54 indicate the results under the condition of CASE-8. In this case, the oscillation is also observed. However, the difference from the CASE-7 appears at the time about 750. A very large vibration occurs and the oscillation has started.

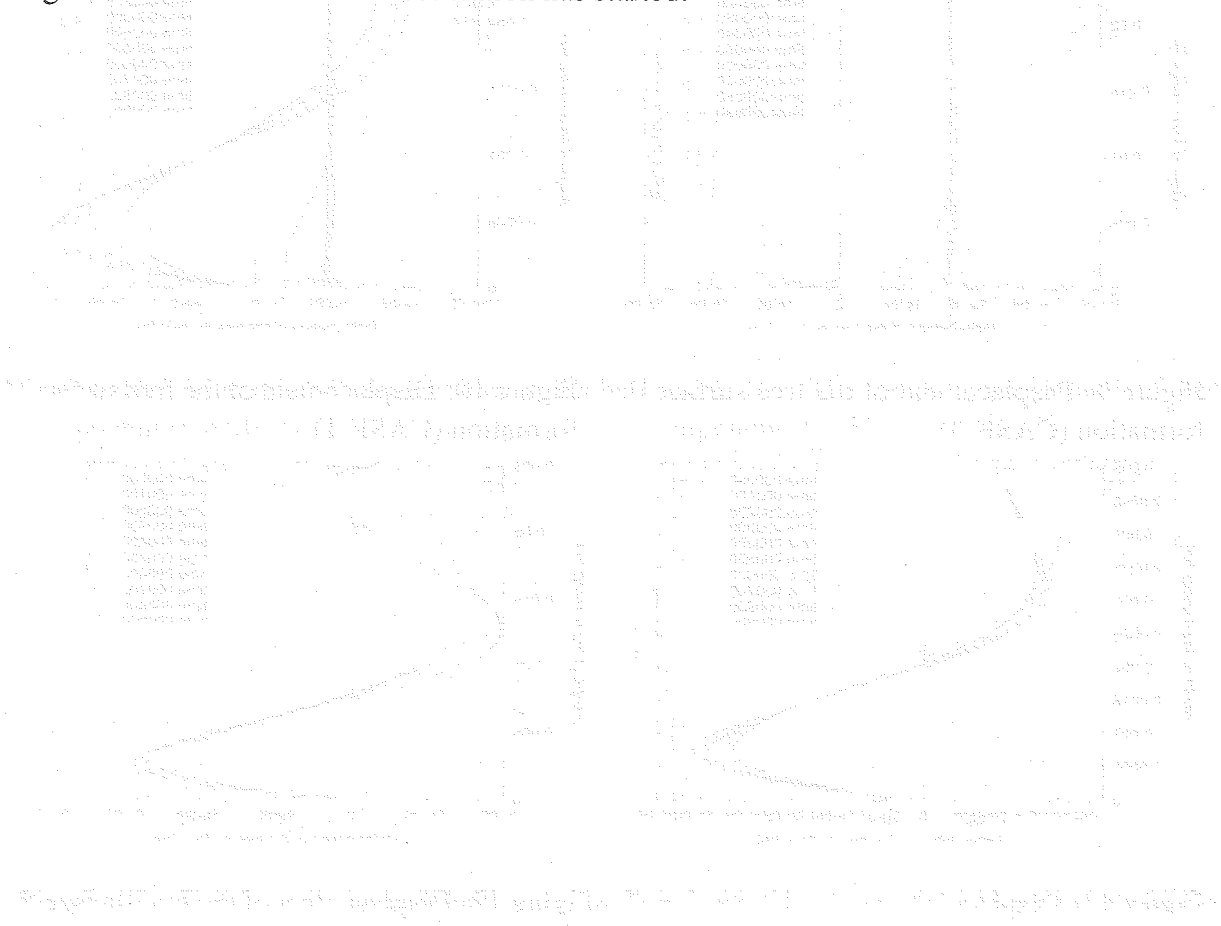

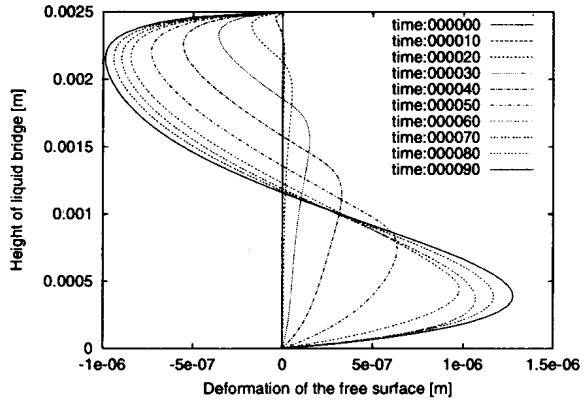

Figure 7: Displacement of the free surface deformation (CASE-1)

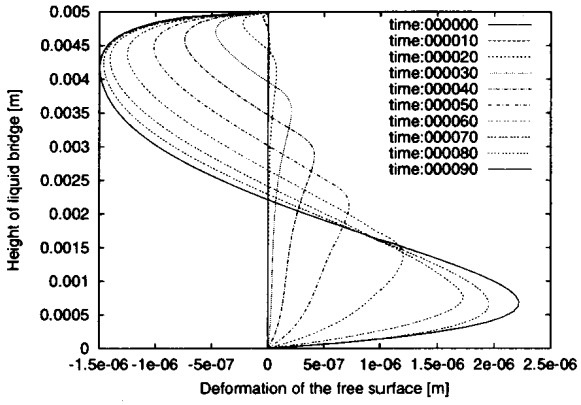

Figure 8: Displacement of the free surface deformation (CASE-2)

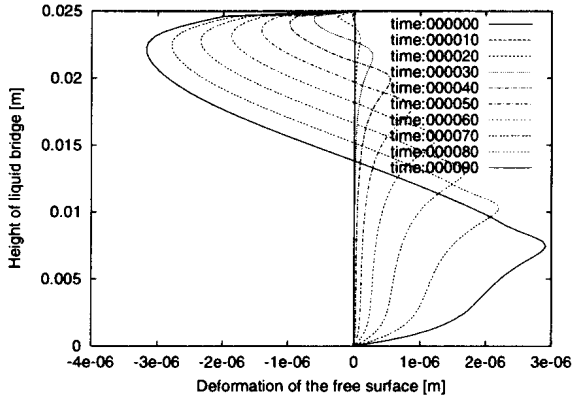

Figure 9: Displacement of the free surface deformation (CASE-3)

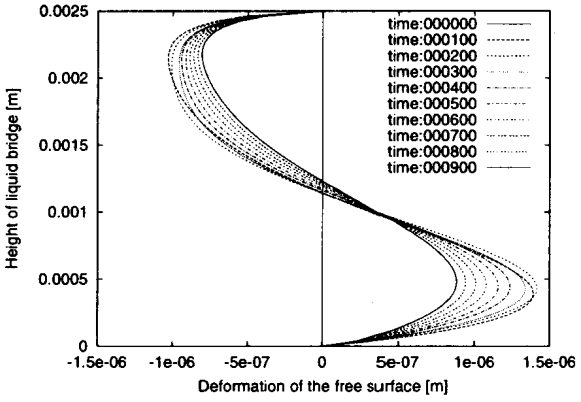

Figure 10: Displacement of the free surface deformation (CASE-1)

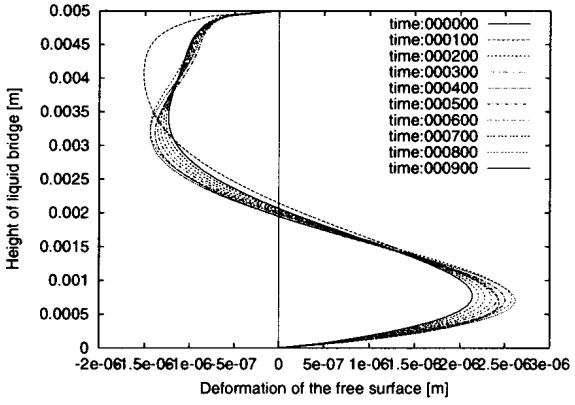

Figure 11: Displacement of the free surface deformation (CASE-2)

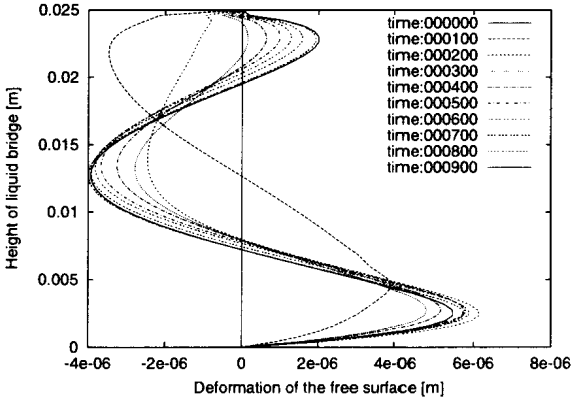

Figure 12: Displacement of the free surface deformation (CASE-3)

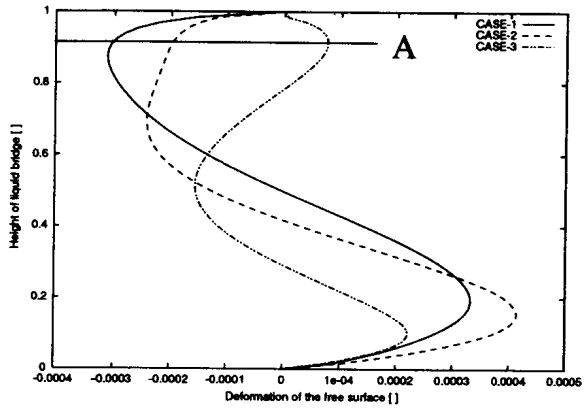

Figure 13: Free surface deformation in the steady state (CASE 1-3)

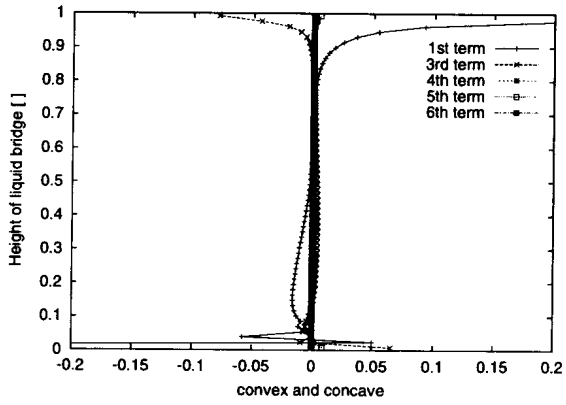

Figure 14: The relative magnitude of each component (CASE-1)

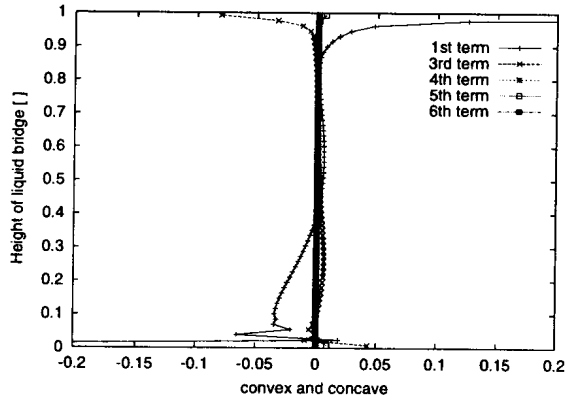

Figure 15: The relative magnitude of each component (CASE-2)

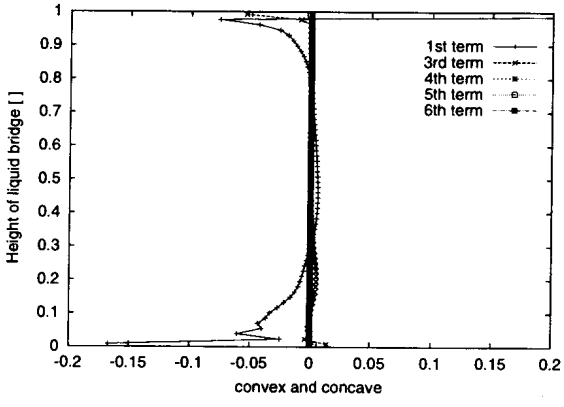

Figure 16: The relative magnitude of each component (CASE-3)

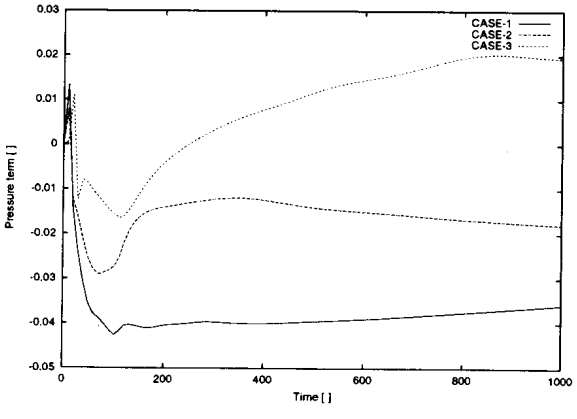

Figure 17: Variation of the pressure and normal stress (CASE 1-3)

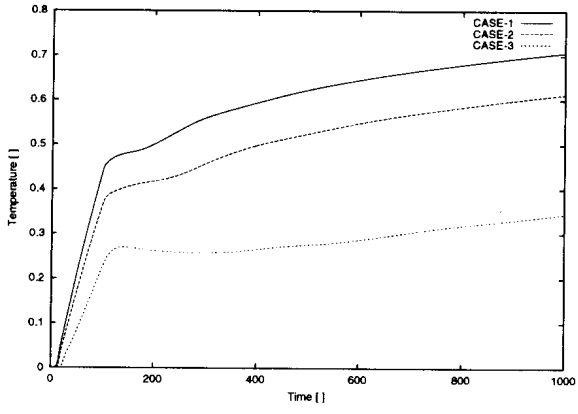

Figure 18: Variation of the temperature on the free surface (CASE 1-3)

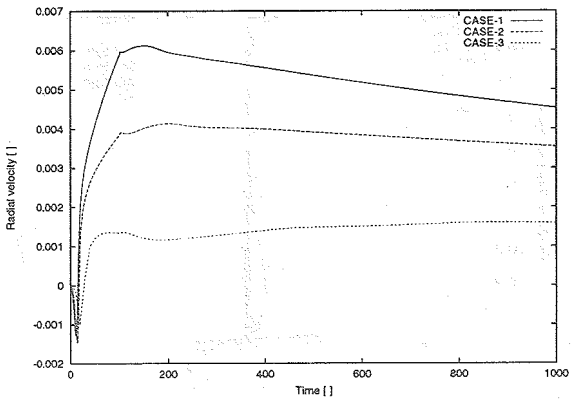

Figure 19: Variation of the radial velocity on the free surface (CASE 1-3)

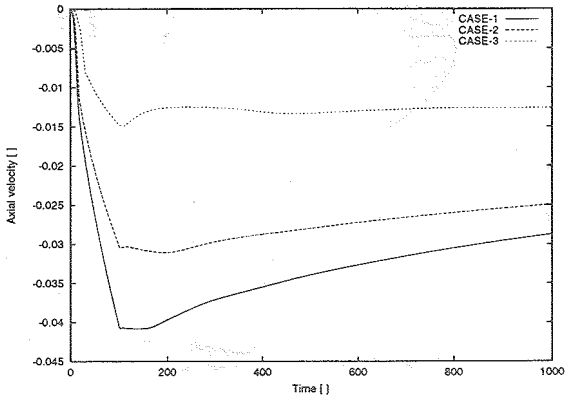

Figure 20: Variation of the axial velocity on the free surface (CASE 1-3)

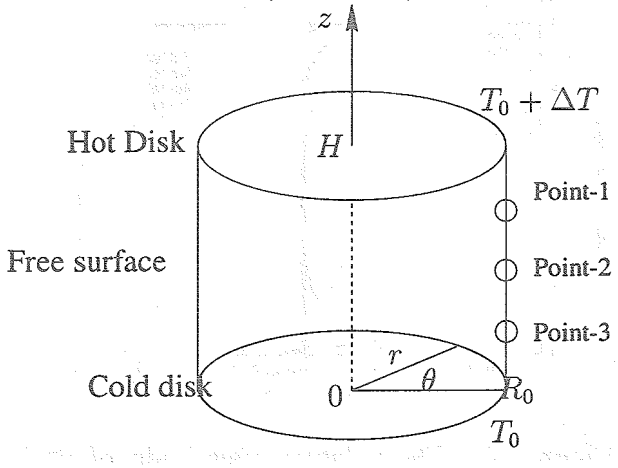

Figure 21: Plotted points

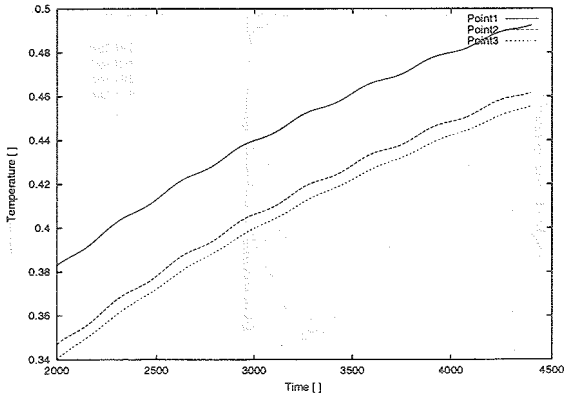

Figure 22: Variation of the free surface temperature (CASE-3)

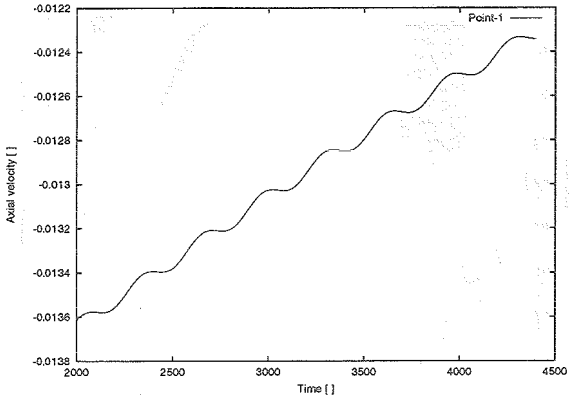

Figure 23: Variation of the axial velocity on the free surface in CASE-3 (Point-1)

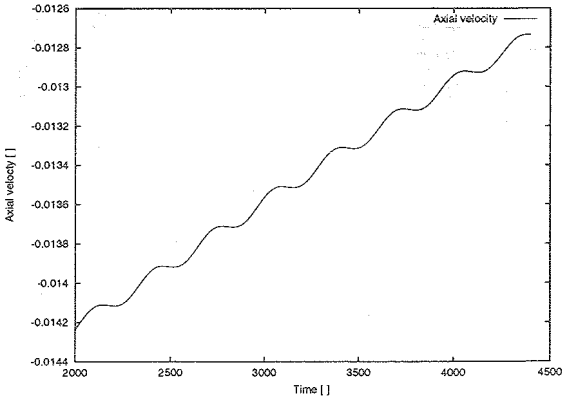

Figure 24: Variation of the axial velocity on the free surface in CASE-3 (Point-2)

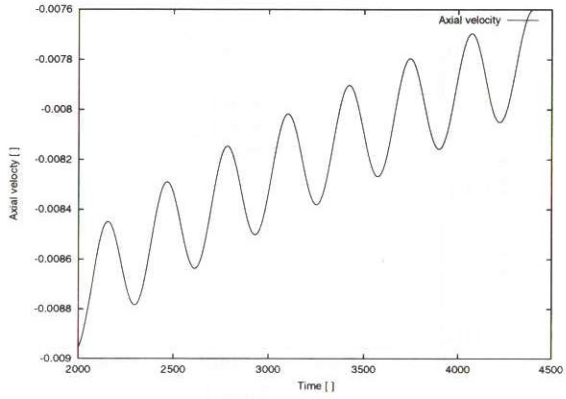

Figure 25: Variation of the axial velocity on the free surface in CASE-3 (Point-3)

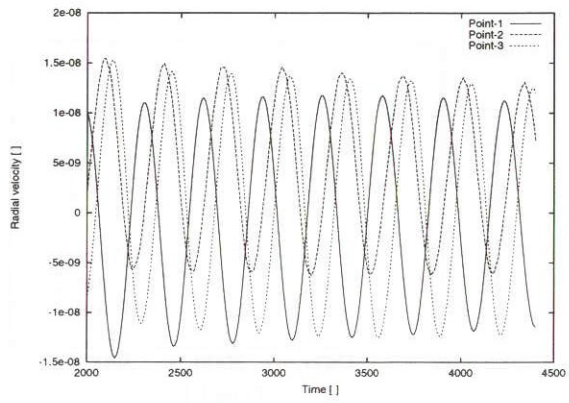

Figure 26: Variation of the radial velocity on the free surface in CASE-3

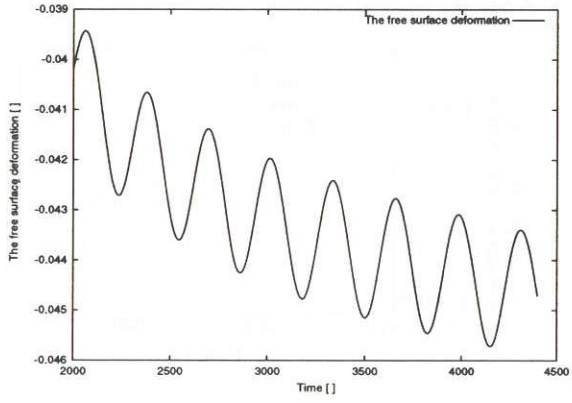

Figure 27: Displacement of the free surface deformation in CASE-3 (Point-1)

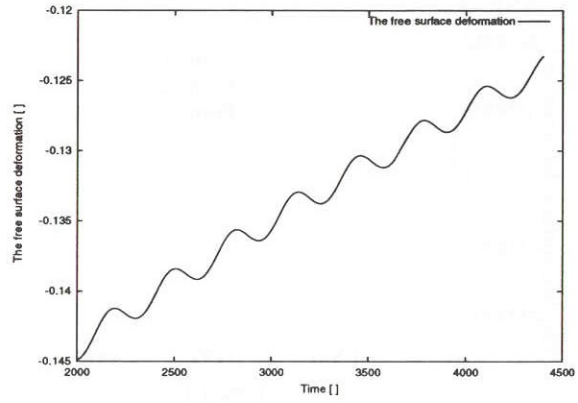

Figure 28: Variation of the free surface deformation in CASE-3 (Point-2)

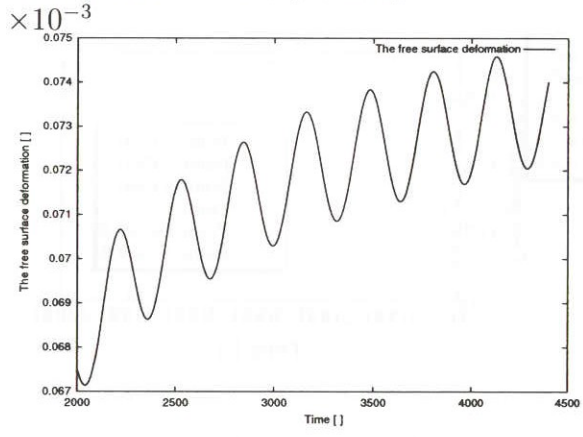

Figure 29: Variation of the free surface deformation in CASE-3 (Point-3)

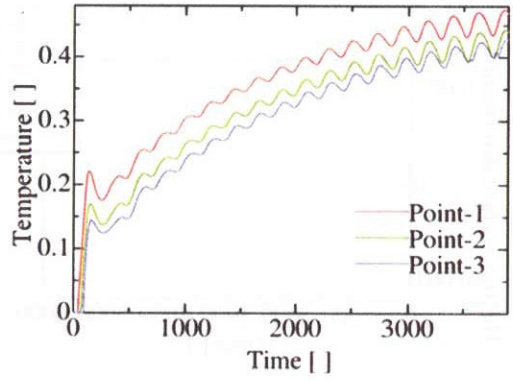

Figure 30: Variation of the free surface temperature in CASE-4

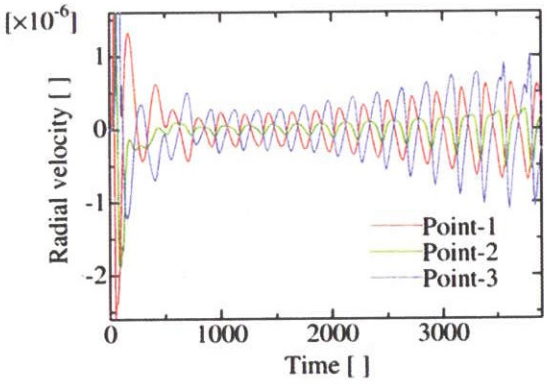

Figure 31: Variation of the radial velocity in CASE-4

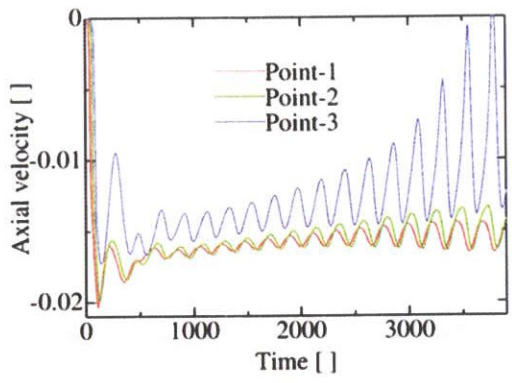

Figure 32: Variation of the axial velocity in CASE-4

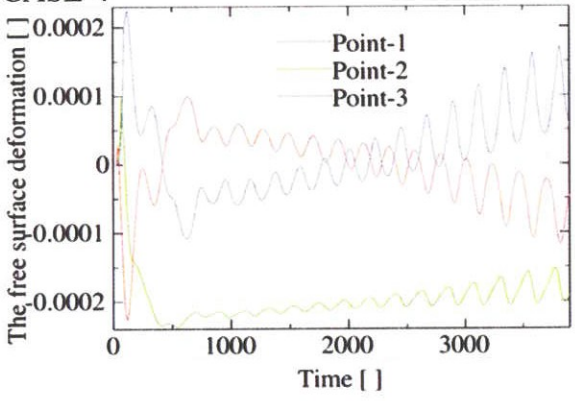

Figure 33: Variation of the free surface deformation in CASE-4

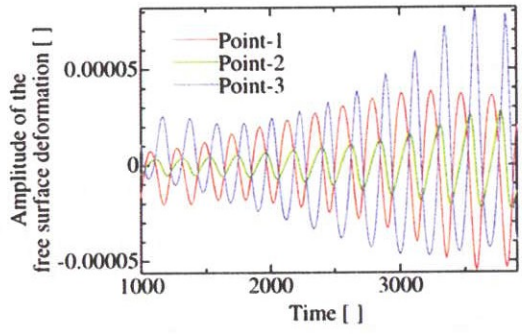

Figure 34: The oscillation amplitude of the free surface in CASE-4

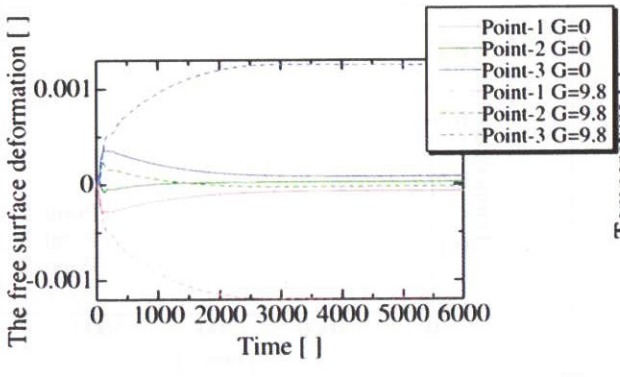

Figure 35: Variation of the free surface deformation (CASE-5 and 6)

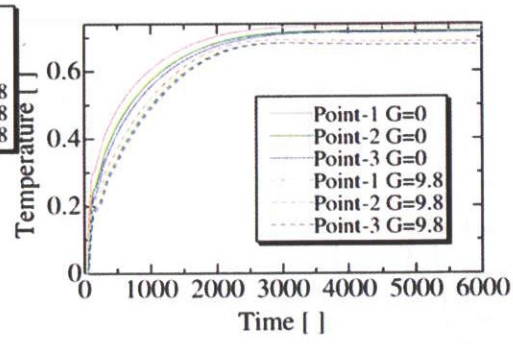

Figure 36: Variation of the free surface temperature (CASE-5 and 6)

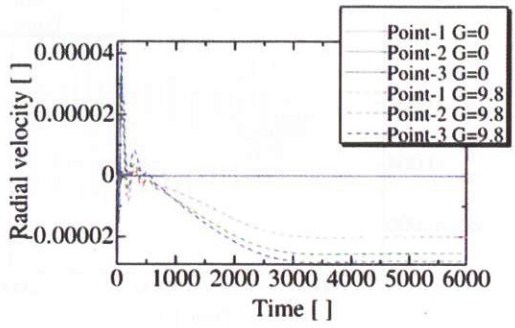

Figure 37: Variation of the axial velocity (CASE-5 and 6)

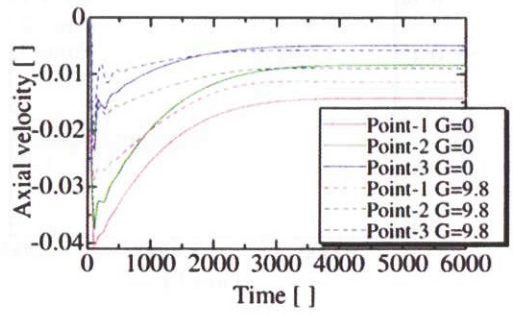

Figure 38: Variation of the radial velocity (CASE-5 and 6)

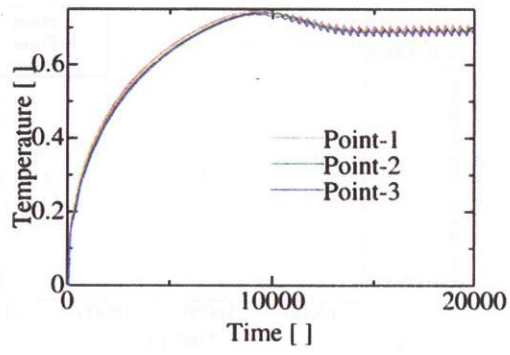

Figure 39: Variation of the free surface temperature (CASE-7)

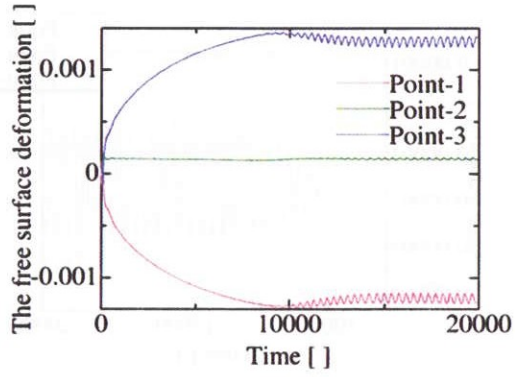

Figure 40: Variation of the free surface deformation (CASE-7)

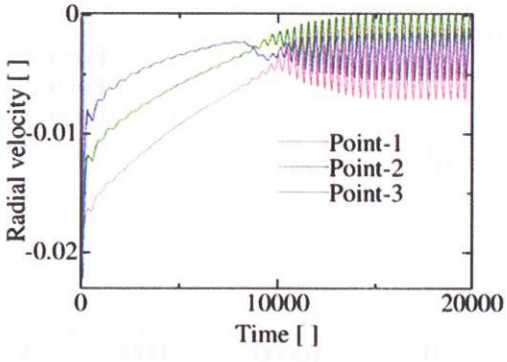

Figure 41: Variation of the radial velocity (CASE-7)

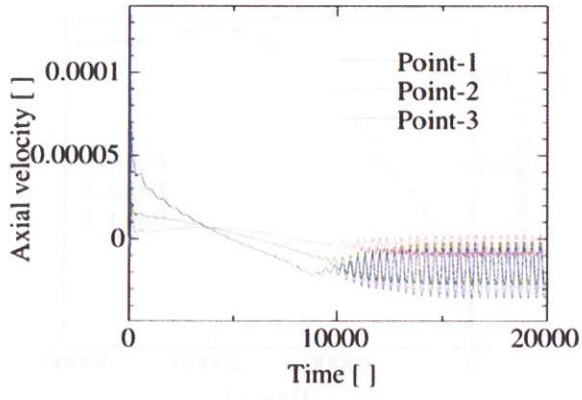

Figure 42: Variation of the axial velocity (CASE-7)

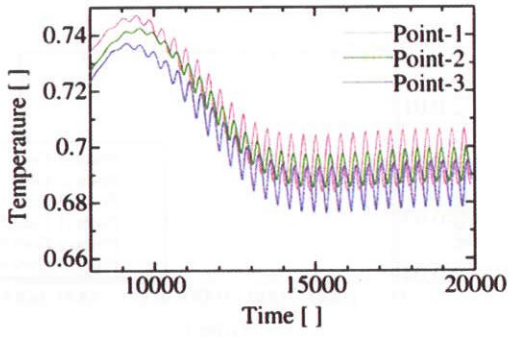

Figure 43: Variation of the free surface temperature (CASE-7)

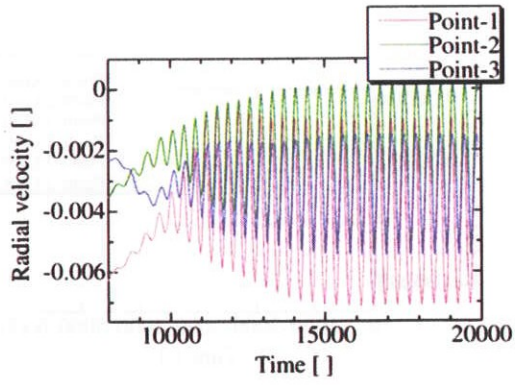

Figure 44: Variation of the radial velocity (CASE-7)

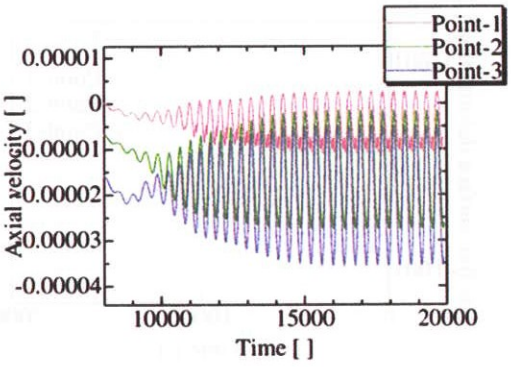

Figure 45: Variation of the axial velocity (CASE-7)

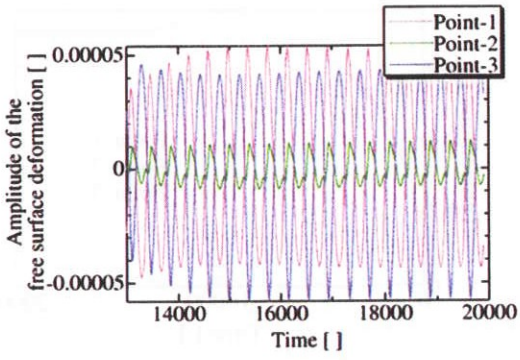

Figure 46: The oscillation amplitude of the free surface (CASE-7)

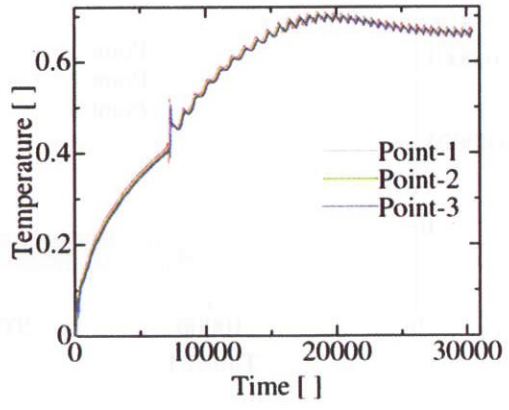

Figure 47: Variation of the free surface temperature (CASE-8)

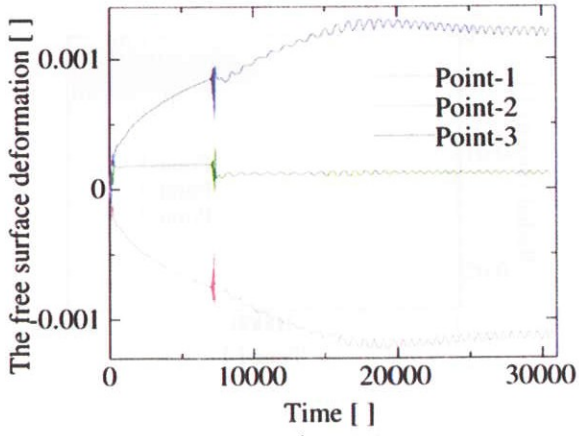

Figure 48: Variation of the free surface deformation (CASE-8)

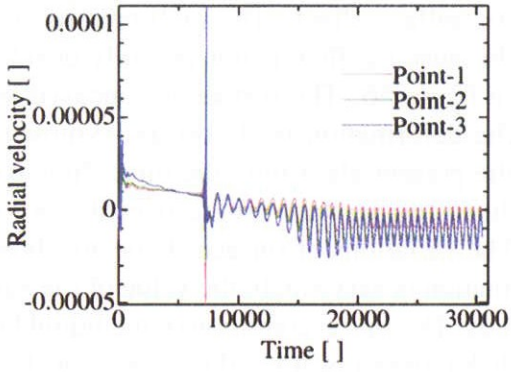

Figure 49: Variation of the radial velocity (CASE-8)

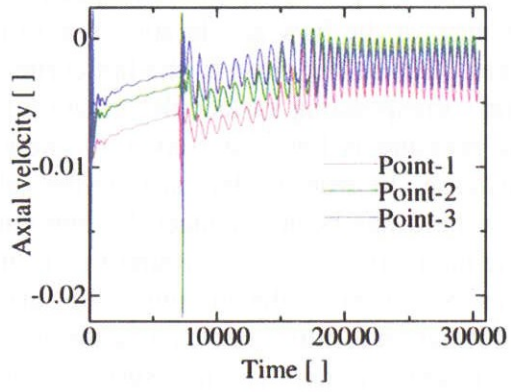

Figure 50: Variation of the axial velocity (CASE-8)

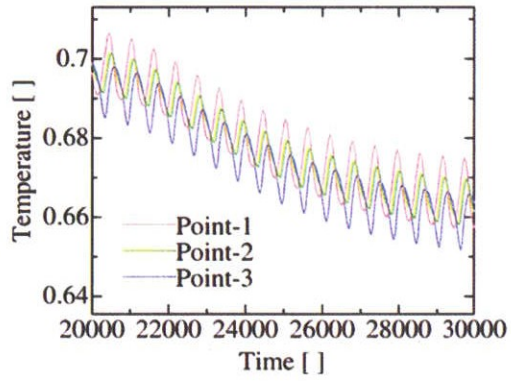

Figure 51: Variation of the free surface temperature (CASE-8)

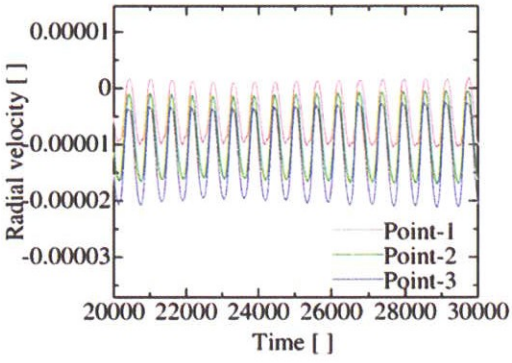

Figure 52: Variation of the radial velocity (CASE-8)

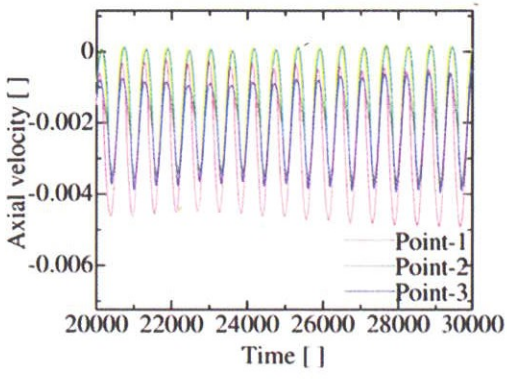

Figure 53: Variation of the axial velocity (CASE-8)

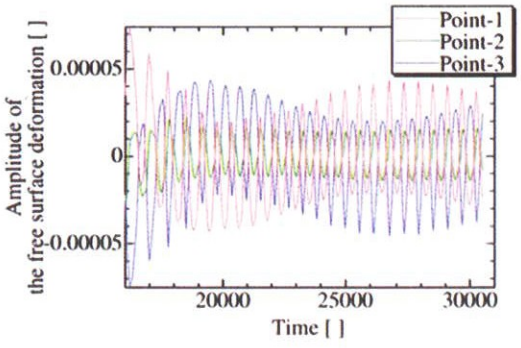

Figure 54: The oscillation amplitude of the free surface (CASE-8)

4.2 Three dimensional calculation on high Prandtl number fluid

The above formulations have been applied to the three dimensional liquid bridge. Calculate conditions are $Ma = 27000$, $Ca = 0.08$, $Pr = 28$, $Bo = 0$, $Gr = 0$. Figure 55 shows the velocity vector ans the pressure in three-dimensional analysis. Red and purple rings indicate the high and low pressure regions, respectively. The low pressure region appears near the hot corner because of the flow acceleration due to the thermocapillary effect. The high pressure region takes place rather close to the hot corner. This is because the flow is not yet fully developed. The corresponding surface deformation is shown in figure 56. The surface is concaved where the pressure is low and convexed where high. The deformation is almost axi-symmetric in this case. In order to demonstrate the validity of the present algorithm, the three dimensional flow field has been enhanced by applying an inclined temperature profile over the hot disk. The inclination is $\pm 50\%$ around the mean value. The variations of surface shape are shown in Figs. 57-59. Since the amount of the surface deformation is very small, the value of the surface deformation is multiplied by a factor of five thousands. The initial condition of the liquid bridge is straight cylinder. The free surface near the hot disk moves inward and the one near the cold disk moves outward. This free surface movement corresponds to the pressure distribution. The order of the displacement is about $0.1 \mu m$ in maximum if the diameter of the liquid bridge is 5 mm.

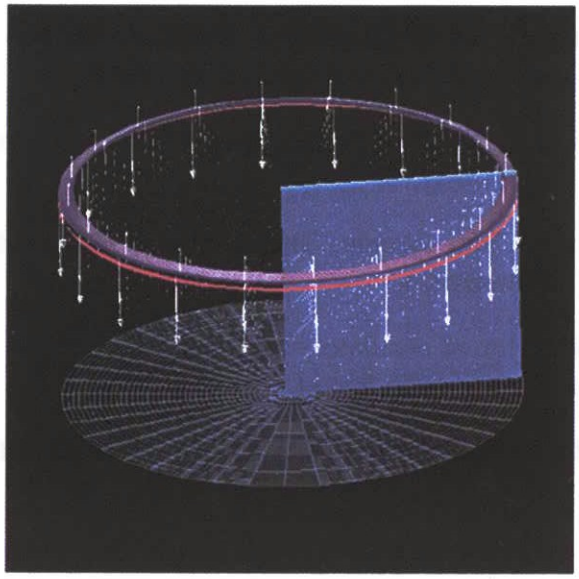

Figure 55: Velocity vector and the pressure in three-dimensional analysis

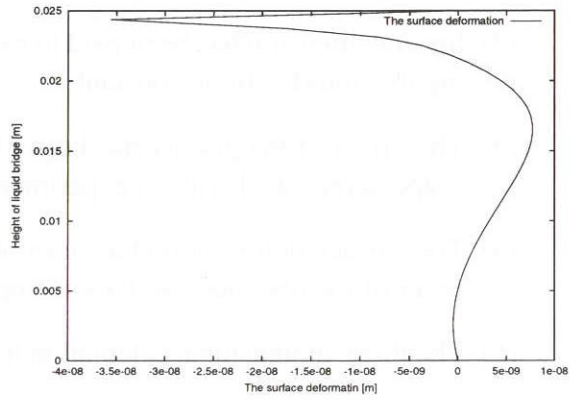

Figure 56: The free surface deformation of three dimensional analysis

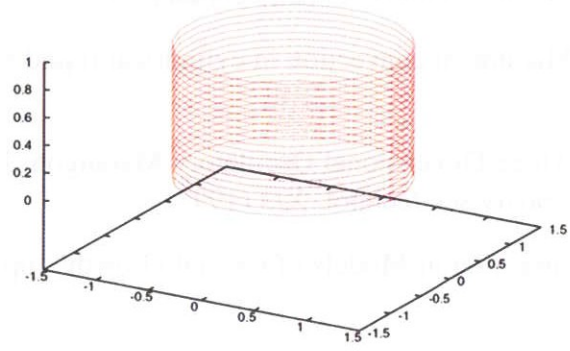

Figure 57: The free surface shape on the three-dimensional analysis (Time=0 [-])

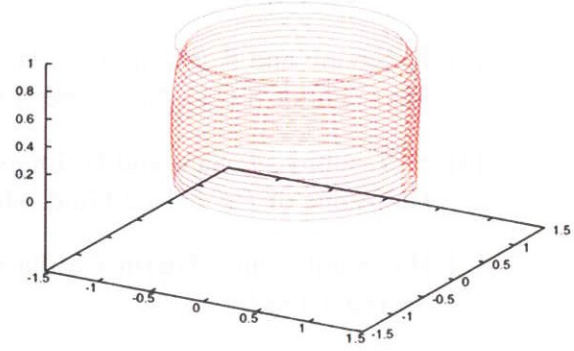

Figure 58: The free surface shape on the three-dimensional analysis (Time=30 [-])

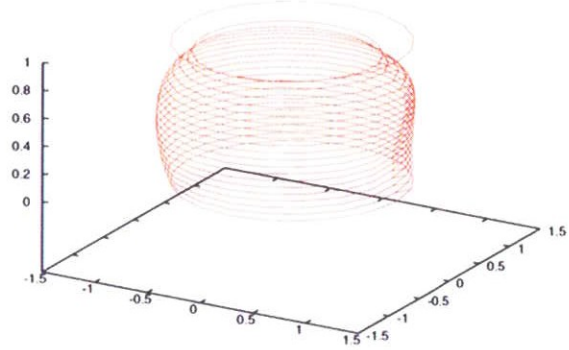

Figure 59: The free surface shape on the three-dimensional analysis (Time=60 [-])

5 CONCLUSIONS

(1) The fundamental equations and the boundary conditions were presented for the two and three dimensional thermocapillary flow with inclusion of the surface deformation.

(2) Spacial attension has been paid to calculate the dynamic surface deformation while keeping the liquid volume constant.

(3) The effect of the gravity has been also taken into account. The calculated static surface shape agrees well with an experimental measurement.

(4) The surface deformation has been obtained for an oscillatory two-dimensional flow. An order of the obtained oscillation amplitude agrees with that of the experiment.

(5) The three-dimensional calculation has demonstrated the validity of the present algorithm.

6 REFERENCES

[1] Y. Kamotani and J. Kim, Effect of zone rotation on oscillatory thermocapillary flow in simulated floating zones, Journal of Crystal Growth 87 (1988) 62-68.

[2] R. Veltan, D. Schwabe and A. Scharmann, The periodic instability of thermocapillary convection in cylindrical liquid bridges, Phys. Fluids A3 (2), February 1991.

[3] R. Savino and R. Monti, Oscillatory Marangoni convection in cylindrical liquid bridges, Phys. Fluids 8 (11), November 1996.

[4] S. Yasuhiro, T. Sato and N. Imaishi, Three Dimensional Oscillatory Marangoni Flow in Half-zone of $Pr = 1.02$ Fluid, Microgravity sci. technol. X/3 (1997)

[5] H.C.Kuhlmann, "Thermocapillary Convection in Models of Crystal Growth", pp.11-18, Springer 1999.